Title
THE SPECTROMETRIC DETERMINATION OF SOME BETA PARTICLE AND CONVERSION ELECTRON ENERGIES

Author
O'Kelley, Grover D.

Publication Date
1951-05-13

UCRL -1243
Cy 2

UNIVERSITY OF CALIFORNIA

Ernest O. Lawrence Radiation Laboratory

BERKELEY, CALIFORNIA

DISCLAIMER

UCRL-1243
MAY 1 5 1951

ag 3

THE SPECTROMETRIC DETERMINATION OF SOME BETA PARTICLE AND CONVERSION ELECTRON ENERGIES

By

Grover Davis O'Kelley

A. B. (Howard College) 1948

DISSERTATION

Submitted in partial satisfaction of the requirements for the degree of

DOCTOR OF PHILOSOPHY

in

Chemistry

in the

GRADUATE DIVISION

of the

UNIVERSITY OF CALIFORNIA

Approved:

.....

.....

.....

Committee in charge

Deposited in the University Library .....
Date Librarian

TABLE OF CONTENTS

THE SPECTROMETRIC DETERMINATION OF SOME BETA PARTICLE AND CONVERSION ELECTRON ENERGIES

Grover Davis O'Kelley
Radiation Laboratory and Department of Chemistry
University of California, Berkeley, California

ABSTRACT

A double focusing beta spectrometer having a radius of 25 cm has been constructed. The theoretical transmission for a resolving power of 1 1/3 percent is about 1 percent of 4π. The spectrometer and auxiliary equipment are described.

The decay of Am^{242} has been investigated, using the beta spectrometer, and a decay scheme is postulated. Schemes are also proposed for the decay of Am^{241}, Cm^{242}, Np^{236}, and Pb^{203}. The radiations of the heavy nuclides Np^{234}, Pu^{243}, Pu^{238}, Pb^{209}, and Pb^{200} have also been measured.

The radiations from neutron deficient isotopes of zirconium and their decay products have been determined, and a decay scheme is postulated for the decay of Zr^{87}.

THE SPECTROMETRIC DETERMINATION OF SOME BETA PARTICLE AND CONVERSION ELECTRON ENERGIES

Grover Davis O'Kelley
Radiation Laboratory and Department of Chemistry
University of California, Berkeley, California

I. INTRODUCTION

In recent years the spectroscopy of radioactive nuclides has become one of the most fruitful fields of nuclear research. Spectrometric measurements of energies and intensities are necessary to test our present concepts of α, β, and γ processes, and further development along theoretical lines is hindered by the fact that relatively few investigators have used such a precise approach to the study of radioactive disintegrations. According to the Table of Isotopes of Seaborg and Perlman[1] there are more than 700 radioactive nuclides known, yet Mitchell's review of disintegration schemes[2] compiles only about 50 which are reasonably well known in the region below lead. Thus, there is a need for careful spectrometric work, rather than the less reliable absorption methods usually employed.

Spectrometric measurements are particularly useful in the heavy region, since these isotopes frequently decay in several different ways, and if some experimentally determined disintegration energies are available, others may be calculated through the use of closed decay cycles. This method has proved very useful in extending the information on electron capture decays. The systematics of alpha radioactivity[3,4] have been a valuable aid in obtaining unmeasured disintegration energies, and have made it possible to predict the radioactive properties of unknown species. By the use of such methods important advances in the study of heavy nuclei have been made, the most noteworthy being the

rather complete and consistent picture of the energy surface in the heavy region[3,4] which has been constructed.

However, the available data on beta disintegration energies leave much to be desired, and it is of considerable importance to measure such schemes with precision comparable to that obtainable in the measurement of alpha particle energies, if unknown energies are to be calculated precisely. The usual beta ray spectrometer is also very useful for making measurements of gamma energies, as described below. Once sufficient data are compiled on the decay schemes of electron capture isotopes, it will perhaps be possible to make the systematics of electron capture decay of Thompson[5] more quantitative, since one would have available the comparative half-lives and electron capture transition energies, if the total decay energy were known from a decay cycle and the daughter energy levels were known from the decay scheme.

It has become customary to call instruments for studying the electron spectra of radioactive isotopes "beta ray spectrometers." Since these devices also yield information about gamma rays by measuring the internally or externally converted electrons, the name "nuclear spectrometer" has been used by Langer and Cook.[6] Before discussing these instruments further, it seems well to describe briefly the theories of beta decay and gamma emission.

Beta disintegration is considered to be a complex transformation of a neutron into a proton or vice versa, with the simultaneous emission or absorption of an electron and neutrino. The theory was developed in its simplest form by Fermi,[7] who used the Heisenberg concept that the

neutron and proton are different states of the same particle. It is postulated that the neutron and proton interact with the combined fields of electron and neutrino in such a way that an electron is created and a neutrino radiated when a neutron changes to a proton. Conversely, a positron and neutrino are radiated when a proton changes to a neutron.

The probability for the emission of a beta particle with momentum between η and $\eta + d\eta$ is given by Fermi as

$$P(\eta)d\eta = G^2/2\pi^3 |M|^2 F(Z,\eta)\eta^2(\varepsilon_o - \varepsilon)^2 d\eta,$$

where η is the momentum of the electron in units of $m_o c$, ε is the total energy in units of $m_o c^2$, and ε_o is the maximum energy of the distribution. The quantity $(\varepsilon_o - \varepsilon)$ represents the momentum and energy of the neutrino. The factor G is given by

$$G = (g/m_o c^2)(m_o c/\hbar)^3,$$

where the constant g measures the strength of the interaction between the nucleons and the electron-neutrino field, and is analogous to e in the quantum electrodynamic treatment of the interaction of electrons with the electromagnetic field (light). This "Fermi constant," g, must be determined empirically.

The factor $|M|^2$ represents the square of the matrix element containing the wave functions of the initial and final states of the neutron and proton and the form of the interaction. For allowed transitions this factor is of the order of unity, but is smaller for forbidden transitions, and may sometimes be dependent upon the energy of electron and neutrino. This behavior arises from the expansion of the matrix element into a series of terms, which become successively smaller if they

do not vanish; only the first nonvanishing term is important to the order of the transition. If the first term does not vanish it is close to unity, regardless of the interaction type and energy. Such transitions are allowed.

For certain transitions the initial and final nuclear wave functions are such that the first term in the M-expansion is zero. In such cases the second term assumes importance, and the transition is first-forbidden. Since successive terms in the expansion decrease by the factor $\bar{\eta}R$, where $\bar{\eta}$ is the average momentum and R is the nuclear radius in units of $\hbar/mc$, the square of the matrix element for first forbidden transitions is smaller by 10^{-2}.

Of the five relativistically invariant forms of the interaction, the tensor and axial vector forms seem to best fit the experimental data. Such interactions lead to the Gamow-Teller selection rules:[8]

$\Delta I = 0, \pm 1$, no $0 \longrightarrow 0$; no parity change (allowed)

$\Delta I = 0, \pm 1, \pm 2$; parity change (1st forbidden)

$\Delta I = 0, \pm 2, \pm 3$; no parity change (2nd forbidden)

Wigner[9] has modified the selection rule by dividing the allowed transitions into "favored" and "unfavored" transitions. The favored transitions are thought to be those in which both parent and daughter nuclei have the same spacial wave-functions. The unfavored transitions then become characterized by a lower matrix element due to a change in the spacial wave functions with respect to symmetry or configuration. In terms of ft values discussed below, the favored transitions would have ft $\sim$3000, while the unfavored ones would have ft $\sim 10^5$. From empirical data alone, the classifications of allowed (unfavored) and

first forbidden transitions thus overlap. The nuclear shell model of Feenberg and Hammack[10] is sometimes helpful, since parities are obtainable from the shell theory.

The decay constant for a transition is obtained by integrating the momentum probability distribution from zero to η_{max}, or

$$\lambda = \ln 2/t_{1/2} = \int_0^{\eta_{max}} P(\eta)d\eta = G^2/2\pi^3 |M|^2 f(Z,\varepsilon_o)$$

where $f(Z,\varepsilon_o) = \int_0^{\eta_{max}} F(Z,\eta)\eta^2(\varepsilon_o - \varepsilon)^2 d\eta$. Since $f(Z,\varepsilon_o)$ is dependent only on the charge and maximum energy, it can be calculated for any isotope for which these quantities are known. The product of f and the half-life in seconds, usually denoted ft, is a measure of the magnitude of $G^2/2\pi^3|M|^2$, and enables one to classify beta transitions as to their orders of forbiddenness. Values of ft fall into groups in which each degree of forbiddenness increases ft by a factor of 100. A very good review of beta decay theory and compilation of ft values is given by Konopinski,[11] while more up-to-date tables of ft values have been compiled by Feenberg and Hammack,[10] and Nordheim.[12] The calculation of $f(Z,\varepsilon_o)$ has been treated recently by Feenberg and Trigg.[13]

Experimental comparison of a momentum distribution with the theory is best done with the aid of a Fermi-Kurie plot,[14] which also yields the maximum energy. If the experimental distribution $N(\eta)$ is expressed as particles per unit time for a constant momentum interval, then

$$N(\eta) \propto P(\eta).$$

For a given type of interaction the factor $G/2\pi^3$ will be constant; the matrix element will also be constant over the distribution except for special forbidden transitions whose matrix elements are energy dependent. These cases are rare, and it will be seen that the Fermi-Kurie plot serves to detect such situations. Therefore, we may write the following equation for a beta spectrum having an allowed shape:

$$N(\eta) = (\text{const})\, F(Z,\eta)\eta^2 (\varepsilon_o - \varepsilon)^2$$

The Fermi-Kurie plot of $N(\eta)/\eta^2 F(Z,\eta)^{1/2}$ as a function of ε is a straight line with an intercept at $\varepsilon = \varepsilon_o$. The units of N, η, and ε do not influence the maximum kinetic energy one obtains from ε_o, so that instead of η, one might use H, $H\rho$, or magnet current of a beta ray spectrometer, and the plot could very well be a function of E in Mev, yielding the maximum kinetic energy E_o directly. However, relativistic units are usually quite convenient.

Use of the Fermi-Kurie plot requires precise knowledge of the form of the function $F(Z,\eta)$. This coulomb correction factor, which is the Dirac wave function for an unbound charged particle in a coulomb field, was given by Fermi[7] in his original article on beta decay. Omitting momentum-independent factors, which do not affect the shape of the Fermi-Kurie plot, this function is:

$$F(Z,\eta) = (\text{const.})\eta^{2S} e^{\pi\nu} \left|\Gamma(1 + S + i\nu)\right|^2,$$

where $S = (1 - \gamma^2)^{1/2} - 1$

$$\gamma = \begin{cases} Z\alpha = Z/137 \text{ for } \beta^- \text{ emission} \\ -Z\alpha = -Z/137 \text{ for } \beta^+ \text{ emission} \end{cases}$$

$$\nu = \left(\gamma\left[1 + \eta^2\right)^{1/2}/\eta\right] = (\gamma)(\varepsilon/\eta)$$

There are no complete tables of the complex gamma function, and so a direct evaluation must be by means of series. To avoid the tedium of

such computations, various approximations have been made. The most reliable approximation is due to Bethe and Bacher:[15]

$$F(Z,\eta) = (\text{const.}) \frac{2\pi\gamma}{1 - e^{-2\pi\gamma}} \left[(1 + \eta^2)(1 + 4\gamma^2) - 1\right]^S$$

This approximation is good to about 3 percent below atomic number 80, and is still the best approximation at atomic number 90, although the error is about 5 percent. However, it is the variation in the percentage error with momentum, and not a constant error which would distort the shape of a Fermi-Kurie plot.

Feister[16] reports a program of computation and tabulation of the exact function $f(Z,\eta) = \eta^2 F(Z,\eta)$ under way at the National Bureau of Standards. It is planned to compute $f(Z,\eta)$ for both negatrons and positrons for all values of η from 0.050 to 7.00 (0.67 to 3100 Kev) at sufficiently close intervals so that intermediate values of η may be directly interpolated. Feister's report includes some of the preliminary results at intervals of 10 Z, up to Z = 90.

Although the Fermi theory is derived on the basis of a simple beta transition, the Fermi-Kurie plot may be resolved into components, if several components are present in the decay. If two components are present, the plot of the high energy one will be a straight line beyond the upper limit of the softer component, but the Fermi-Kurie plot of the mixture will rise above the straight line at energies below the maximum energy of the soft component. The straight line obtained by extrapolating the hard component to lower energies is subtracted from the curve of the mixture, recalling that the Fermi-Kurie plot of the soft component is $\sqrt{(N_{total} - N_o)/\eta^2 F}$ against , where N_o is

obtained from the extrapolated high energy component. However, such a procedure should be used with caution, since scattering from the source and spectrometer walls can cause an excess of electrons at low energies which may resemble a separate component. If two beta particles decay from the same level in the parent to different levels in the daughter nucleus, the presence of gamma rays will indicate the validity of the resolution into components. End points of lower energy components can generally be obtained with reasonable precision in this way, except where the low energy beta particles are of such low intensity that they must compete with backscattered electrons from the more intense components. It is good practice, therefore, to use very thin samples and backings.

Theoretically, the Fermi-Kurie plot for infinite and finite resolving power will coincide except in the region of the endpoint. In practice, the resolving power is generally dependent upon source thickness, and it is possible for a thick source and poor resolving power to distort a straight-line Fermi-Kurie plot, or to straighten out a curved plot. This is particularly important in cases where small deviations from linearity are significant, as in studies of forbidden spectral shapes. Owen and Primakoff,[17] and Wu and Feldman[18] have studied the effect of poor resolution and thick sources, which in some cases turns out to be quite pronounced.

When a nucleus is left in an excited level as a result of radioactive decay, gamma ray bombardment, or other excitation process, the probability for gamma ray emission to a lower level becomes high. The quantum theory of radiation employs the classical concept of a

radiating source as an oscillating electric or magnetic multipole, and employs instead of the classical frequency ω, the quantity $h\omega$ times the probability that a gamma ray shall be emitted.

Since the radiation carries away angular momentum, application of conservation of momentum to the system of nucleus and photon leads one to establish the following selection rule:

$$|\bar{I} - \bar{I}'| \leq \ell,$$

where $\bar{I}$ and $\bar{I}'$ are the angular momentum vectors in units of $\hbar$ for the states between which an electric or magnetic 2^ℓ pole transition occurs.

The radiation of lowest order (i.e., the most probable) between two levels with angular momenta I and I' will be an electric or magnetic multipole of order 2^ℓ, in which

$$\ell = |I - I'|$$

Note that I and I' are the scalar quantities.

When one also considers parity, i.e., what happens to a given eigenfunction if the sign of all the particle coordinates is changed, the following complete selection rules result:

Order $=\Lambda$	1	2	3	4	5
Electric radiation	Dipole	Quadrupole	Oct.	16-pole	32-pole
ℓ	1	2	3	4	5
Parity change	yes	no	yes	no	yes
Magnetic Radiation	--	Dipole	Quad.	Oct.	16-pole
ℓ	--	1	2	3	4
Parity change	--	no	yes	no	yes

The table also includes values of the order of the transition, denoted by Λ. To the table must be added the selection rule that $0 \longrightarrow 0$ transitions are forbidden for all types of radiation. This is a result of the equation for minimum ℓ given above.

The present state of knowledge of nuclear structure is not sufficient to allow calculation of absolute transition probabilities, but various authors have calculated nuclear lifetimes assuming different nuclear models. Segrè and Helmholz[19] have obtained an approximate formula for the decay constant by simplifying a treatment of the problem due to Bethe:[20]

$$\log_{10}\lambda_\gamma = 20.30 - 2\log_{10}(1\cdot3 \ldots 2\ell - 1) - (2\ell + 1)(1.30 - \log_{10}E) - 2\ell(0.84 - 1/3\log_{10}A,$$

where λ_γ is in sec^{-1}, E is the gamma ray energy in Mev, and ℓ is the multipole order for electric transitions. However, withing the accuracy of such a calculation, the decay constant for 2^ℓ pole magnetic radiation has the same probability as electric $2^{\ell+1}$ pole radiation, the decay constant of magnetic 2^ℓ pole is obtained from the formula by setting $\Lambda = \ell + 1$.

A nucleus may also decay to a lower energy state by giving the energy difference between the two states to an electron in the K, L, M --- shell of the atom. Thus, monoenergetic electrons are ejected with kinetic energies $E_\gamma - E_K$, $E_\gamma - E_L$, etc., where E_γ is the energy difference between the levels, and E_K, E_L, etc. the binding energy of the electrons in their respective shells. Such a process is called "internal conversion." It is important to realize that this is a primary process, for internal conversion competes with gamma ray

emission, and the decay constant for the excited state is the sum of the decay constants for the two processes. Thus,

$$\lambda = \lambda_\gamma + \lambda_e$$

and $T_{1/2} = 0.693/(\lambda_\gamma + \lambda_e) = 0.693/\lambda_\gamma(1 + \alpha)$,

where λ_γ is the decay constant for gamma ray emission, λ_e is the decay constant for the internal conversion process, and α is the internal conversion coefficient, defined as the number of internal conversion electrons per unconverted gamma ray. Axel and Dancoff[21] show that when this correction is applied to an equation for λ_γ having about the same energy dependence as Segrè and Helmholz's equation, very good agreement exists between theory and experiment.

Although the calculation of λ relies upon knowledge of nuclear matrix elements and nuclear structure, the calculation of internal conversion coefficients depends only upon knowledge of electrodynamics and atomic structure. Internal conversion offers a means of exploring the multipole order of transitions, since the degree of conversion depends greatly upon the electric and magnetic field in the vicinity of the nucleus where the K- and L-electrons are located. The field decreases with a power of r which is related to the multipole order. Although the calculation of numerical values is a formidable task, the theoretical evaluation is well known and has been treated by several workers. Hulme[22] has treated internal conversion in the K- and L-shells due to the field of an electric dipole, using Dirac's relativistic equations. Goertzel and Rose[23] have generalized Hulme's treatment to include radiation from multipoles of arbitrary order. An extensive numerical calculation of K-shell conversion coefficients for

electric and magnetic multipole radiation up to order 2^5 has been carried out by Rose and co-workers.[24] Their results have been distributed privately in the form of tables.

The analytic expressions of Goetzel and Rose[23] were simplified from a computational point of view by Gellman and co-workers,[25] who have published preliminary results for the L_I shell only, for the electric dipole, magnetic dipole, and electric quadropole cases. These preliminary results are exact except that screening has been omitted. However, a rough screening correction may be made[19] by replacing Z by (Z-4) when interpolating the curves of Gellman, et al.

As a result of a spectrometric investigation of a radionuclide, the atomic number, gamma ray energy, and ratio of K electrons to L electrons can be determined. If the transition is isomeric, the half-life of the gamma transition can be directly measured. Even if the conversion coefficients cannot be directly measured the half-life and N_K/N_L ratio are very helpful in assigning a multipole order to the transition. Unfortunately, sufficient calculation of conversion coefficients have not been made for the L shell to allow use of the α_K/α_L ratio reliably above an atomic number of about 35.

Some additional aspects of beta decay and gamma ray emission will be discussed in connection with the experimental work described below.

II. APPARATUS

Before describing the beta spectrometer (or "nuclear spectrometer") used in the investigations below, it would be well to recall some general features of magnetic beta spectrometers.

If an electron in an evacuated space moves in a plane perpendicular to a magnetic field H, it will describe a circular path in that plane. The magnetic force $e(\underline{H}x\underline{v})$ on each electron is then balanced by the centrifugal force mv^2/ρ. Therefore one obtains the following relation, which holds relativistically:

$$Hev = \frac{mv^2}{\rho}$$

On rearrangement,

$$p = mv = eH\rho$$

In these equations H is the field in gauss, e is the charge on the electron in emu, ρ is the radius of curvature in cm, and m is the mass of the electron at velocity v.

Since charged particles, such as electrons, often move at right angles to uniform magnetic fields, $H\rho$ values are convenient primary measurements. The "magnetic rigidity" or $H\rho$ is proportional to the relativistic momentum, whence the momentum in units m_oc becomes

$$\eta = \frac{p}{m_oc} = \frac{e}{m_oc} \cdot H\rho = \frac{H\rho(\text{gauss-cm})}{1704.1}$$

After eliminating velocities in the relativistic equations for momentum and energy, one can relate $H\rho$ in gauss - cm and E in Mev as follows:

$$H\rho = 3336 \left[E^2 + 1.022\ E\right]^{1/2}$$

$$E = \left[0.2609 + 8.987 \times 10^{-8}(H\rho)^2\right]1/2 - 0.5108$$

The inverse resolution R of a beta spectrometer is defined as $\Delta p/p$; the "momentum bandwidth" Δp is a measure of the momentum spread of electrons which can strike the detector when the spectrometer is adjusted to focus electrons of momentum p. For a monoenergetic electron

line, R is the halfwidth of the measured line divided by the position of the peak of the line. Thus the inverse resolution is dimensionless; it is independent of momentum for all magnetic spectrometers.

Since the inverse resolution is a constant of the apparatus, and the momentum is proportional to the magnetic rigidity, the momentum bandwidth is proportional to momentum, magnetic rigidity, or to any other measurable quantity that is proportional to momentum:

$$\Delta p = Rp = (Re)H\rho$$

In the analysis of continuous beta spectra it is therefore necessary to divide the counting rate at each momentum setting by some quantity proportional to momentum, so that the activities are normalized to a constant momentum interval.

Beta spectrometers may be conveniently divided into two groups, the flat spectrometers and the helical spectrometers. An example of the former is the semicircular spectrometer proposed by Danysz,[26] which is still widely used. Figure 1 shows such a device, which makes use of a uniform magnetic field perpendicular to the electron beam. The electrons described circular paths, those of equal energy having equal radii. Two electrons diverging from the source S with almost the same initial direction will converge at one and the same point after traversing approximately 180° of arc (point A, Figure 1). The central rays will have the same radius of curvature as the diverging rays, but will strike the image plane at point B of Figure 1. Thus, even for a point source, the resolving power is limited. Electrons leaving the source at angles to the focusing plane of Figure 1 will have reduced

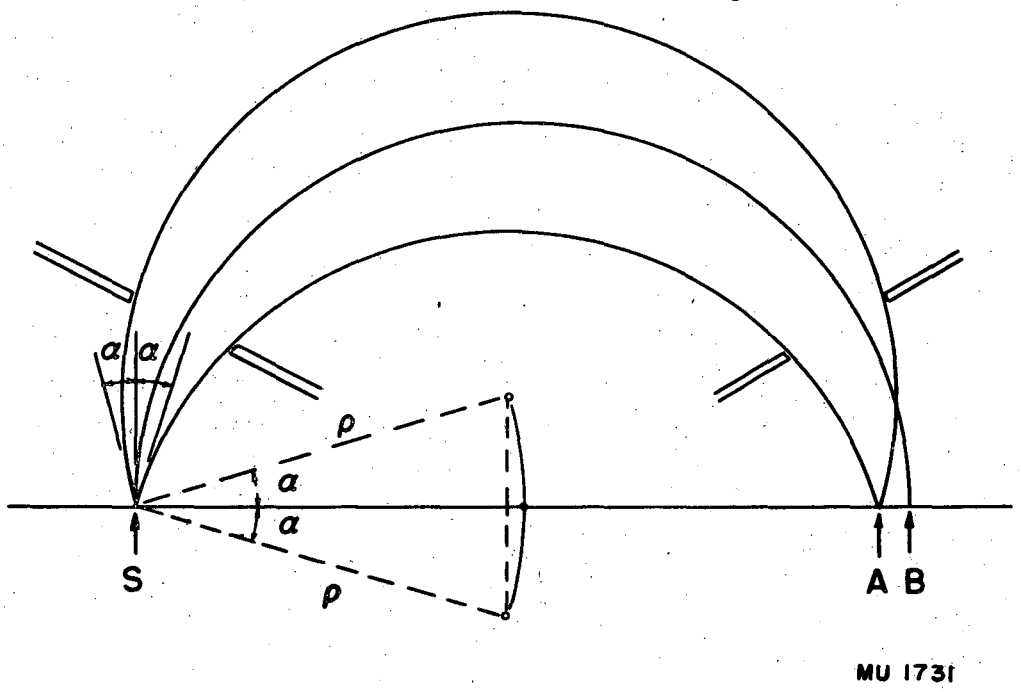

Fig. 1

Electron trajectories in the semicircular beta spectrometer

momentum components in that plane, and their paths projected on the image plane will be circles of shorter radii than the rays shown in Figure 1; this effect will increase the low energy "tail" of a monoenergetic electron line. It will be seen that for this type of beta spectrometer, the conditions that would improve the resolution (narrow beam aperture, source, and exit slit) all serve to decrease the number of electrons reaching the detector, and will reduce the transmission of the instrument. In all beta spectrometers, a compromise is necessary between resolving power and transmission.

The low transmission of the Danysz spectrometer due to its one-dimensional focusing has led to the use of the various helical spectrometers, which utilize the focusing property of an axially symmetric field for electrons emerging from a source located on the axis. The path is a cylindrical helix with the axis parallel to the direction of the field. Such a system forms a convergent magnetic lens. The use of a magnetic lens in beta spectroscopy was proposed by Kapitza,[27] and first accomplished by Tricker.[28] The high transmission of the two-dimensional focusing helical spectrometers is generally counterbalanced by a poorer resolving power than the semicircular instrument. However, recent modifications of helical spectrometers have improved somewhat the relation between transmission and resolving power.

It was shown by Svartholm and Siegbahn that it is possible to combine the advantage of space focusing (high transmission) with that of using central rays (high resolving power). Such a spectrometer may be considered a flat spectrometer derived from the semicircular instrument by replacing the uniform magnetic field by a non-uniform one, in

such a way that there is axial focusing as strong as the radial focusing. Siegbahn, Svartholm, and their co-workers[29-31] have studied the theory of this particular focusing device in considerable detail, while Shull and Dennison[32] have shown such focusing to arise from a general treatment of magnetic spectrometers. E. M. McMillan appears to have first proposed this "double-focusing" spectrometer although his results were not published at that time.

Because of its good transmission and high resolving power, such a double-focusing beta spectrometer has been constructed in this laboratory, and it is the purpose of this paper to describe this instrument and some of the measurements for which it has been used. Before proceeding, a brief review of the theory of this spectrometer will be given.

Consider an inhomogeneous magnetic field of cylindrical symmetry, with a plane of symmetry perpendicular to the axis. According to the theory of the focusing properties of such a field, there is an axial focusing action which decreases outward from the center of symmetry, as well as a radial focusing action if the field does not decrease faster than the reciprocal of the radius from the axis. If the axial component of the field in the median plane at a distance r from the axis is denoted by $H(r)$, and its derivative with respect to r by $H'(r)$, then an electron leaving a point on the circle $r = r_o$ in the median plane and at a small angle to the circle, will strike the cylindrical surface $r = r_o$ after an angle ϕ_r, the radial focusing angle, and the symmetry plane after an angle ϕ_z, the axial focusing angle. These focusing angles are given by:[29]

$$\phi_r = \pi\left[1 + \frac{r_o H'(r_o)}{H(r_o)}\right]^{1/2}$$

$$\phi_z = \pi\left[\frac{- r_o H'(r_o)}{H(r_o)}\right]^{1/2}$$

which yields the relation

$$\frac{1}{\phi_r^2} + \frac{1}{\phi_z^2} = \frac{1}{\pi^2}$$

The radial and axial focusing will be of equal strength if $\phi_r = \phi_z$, which gives $H'(r_o) = - 1/2\ r_o H(r_o)$. Thus, we have an optical axis of radius r_o, on which the object and image are separated by an angle $\pi\sqrt{2}$ radians.

The required field varies approximately as $1/\sqrt{r}$ in the vicinity of the optical axis r_o. It is desirable to define the field shape more closely to focus rays diverging from the optical axis at considerable angles; thus a series expansion of the axial field component in the median plane H(r) is employed:

$$H(r) = H_o\left[1 + \alpha\ \frac{r - r_o}{r_o} + \beta\left(\frac{r - r_o}{r_o}\right)^2 + \ldots\right],$$

where H_o is the axial field component at r_o, r is the radius in the vicinity of r_o, and α and β are constants. From the above expression relating the derivative of the field to the field at $r = r_o$, α must be equal to - 1/2, while the other coefficients are at our disposal. Svartholm,[30] McMillan (private communication to Svartholm and Siegbahn), and Shull and Dennison[32] have all shown that the coefficient β is the factor which determines the aberration and hence the resolution of such a spectrometer. Values of β from 1/8 to 3/8 have been employed;[31,33,34] the choice of β involves practical considerations

of magnet design. Persico and Geoffrion[35] propose the use of $\beta = 3/16$, for which the ratio of transmission to polepiece area is very high.

Figure 2 shows a general layout of a typical double focusing spectrometer. The source and detector are located $\pi\sqrt{2}$ or about 255° apart, and the entrance slit A is midway on the electron trajectories. The divergence angles are determined by this slit; the radial beam width is $2\sqrt{2}\ r_o\gamma_1$ and the axial beam width is given by $2\sqrt{2}\ r_o\gamma_2$.

Svartholm and Siegbahn[29,30] have shown the dispersion of the double focusing spectrometer to be twice that of a semicircular one, and an aberration width about half as large. Also, one obtains the interesting result that for $\beta = 1/8$, the radial defocusing is eliminated, and for $\beta = 3/8$, the same is true for axial defocusing. When γ_1 and γ_2 are about the same, it is impossible to reduce the aberration width by a choice of β between 1/8 and 3/8, but one can improve the resolution through the use of an extended aperture. For example, if $\beta = 1/8$ (as in the instrument below) one should use a large radial acceptance angle and a relatively smaller axial angle which can be varied to obtain various line widths. In such a case, the transmission varies linearly with the axial aperture, while the line width decreases according to a square law.

Two alternative magnet designs are shown in Figure 3. Design (a) allows the use of a large radial extension of the beam, and hence is very suitable for a double-focusing beta spectrometer with $\beta = 1/8$. Also, with this choice of field shape, the polepieces may be placed fairly close together, and fringing effects do not become serious. This magnet is eminently suited to theoretical design, and may be

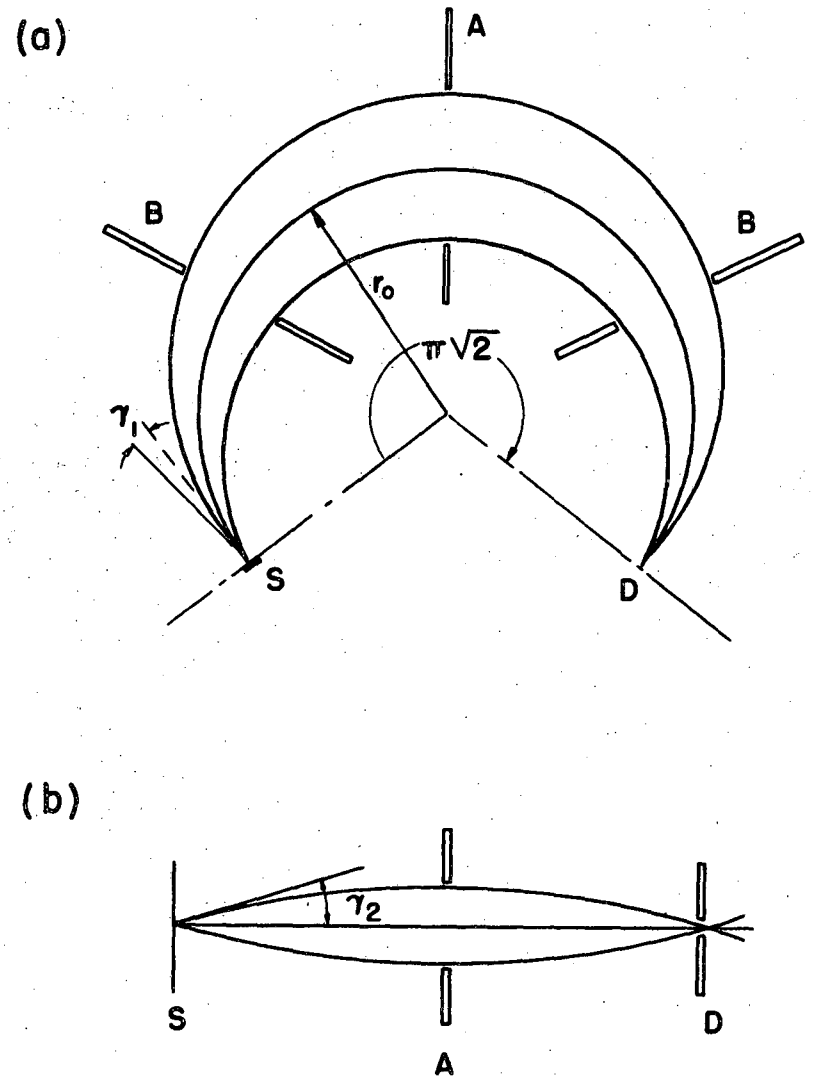

Fig. 2

Double focusing spectrometer: projection of electron paths (a) in the median plane, and (b) in the axial plane

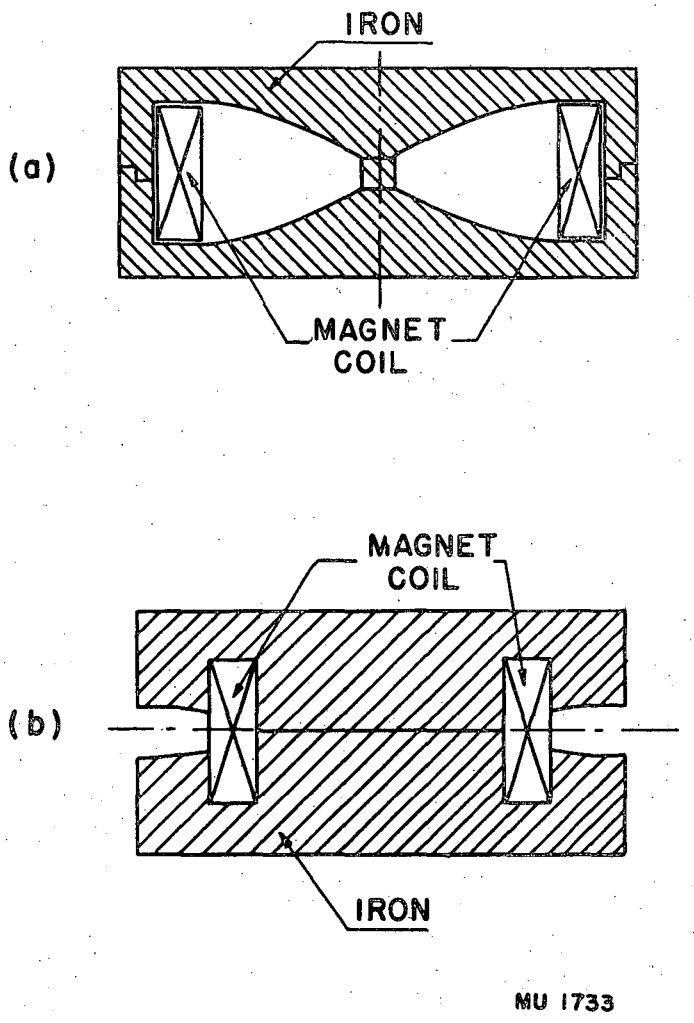

Fig. 3

Alternative magnet designs for the double focusing beta spectrometer

machined to a calculated pole shape with confidence that the magnetic field will have the proper distribution. For these reasons the spectrometer described herein was constructed similar to the closed magnetic circuit spectrometer of Figure 3-(a), even though this design requires more copper and power for the same radius than the instrument shown in Figure 3-(b). The "double mushroom" magnet of Figure 3-(b) is due to Cockcroft[36] who used such an arrangement for a large alpha spectrometer. It has the advantage of yielding large radii with a magnet of modest physical size, but has the disadvantage of a small radial area, because of the magnet coil. Thus, to obtain the optimum transmission a large axial aperture must be used, with the result that a β of 3/8 is required. In this case the polepieces are spaced much farther than in the former instrument, and fringing effects become difficult to cope with except by empirical means.

The polepieces of our spectrometer were carefully designed theoretically, and machined to an average tolerance of better than 0.1 percent in the bending zone. A diagram in cross section for half of one polepiece is shown in Figure 4, together with its theoretical dimensions. Because of the cylindrical symmetry of the device, the other half of the polepiece cross section is the same. The equilibrium radius chosen was 25.00 cm, or 9.842 inches. An assembly drawing, Figure 5, shows the method of mounting the magnet coil, which consists of 725 turns of number 8 Formex insulated wire, having a resistance of 3.95 ohms. The spool upon which the magnet coil is wound is separated from the vacuum tank of the spectrometer by a brass wall, rendered vacuum-tight by rubber gaskets. A small, radar type blower circulates

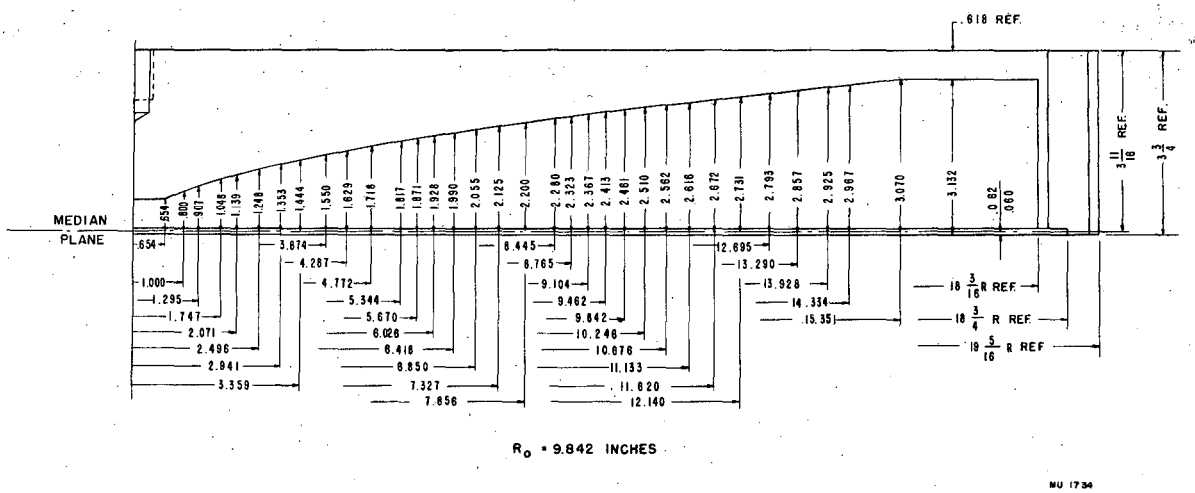

Fig. 4

Cross section of double focusing spectrometer polepiece

air around the magnet coil when the magnet power supply is operated. The temperature of the magnet coil may be estimated by a thermocouple placed inside the winding, but no heating has been observed, even when operating at 10 amperes through the coil. Such a current corresponds to about 18,000 gauss - cm or 5 Mev, and is the limit of the magnet power supply.

As shown in Figure 5, a vacuum tight, brass well is introduced into the spectrometer chamber for making field measurements in the median plane. If it is desired to measure the field in the region on each side of the equilibrium radius, the spectrometer vacuum tank can be let down to atmospheric pressure, and the fluxmeter well may be released and rotated to each side of its normally fixed position. An external pointer is adjusted so the position of the search coil within the well is known precisely. Figure 6 shows the result of such a field shape measurement, and demonstrates the close agreement between the actual field and the theoretical shape. The deviations from the calculated curve at low radii are probably not significant, as the probe position was relatively uncertain there. Deviations below a radius of 8 inches or above 12 inches would only affect the transmission, leaving the resolving power essentially unchanged.

The power supply for the magnet coil is composed of a bridge type selenium rectifier, a low ripple, choke input filter, and a suitable regulating circuit. The operation of the control and stabilizing circuit is as follows. A saturable reactor bank, connected in series with the isolation transformer supplying the selenium rectifier, can be controlled by two pairs of 304 - TL vacuum tubes, so that the voltage

Fig. 5

Assembly drawing of the beta spectrometer

A. Airlock for introducing sample probe

B. Airlock gate valve

C. Airlock pumpout valve

D. Rotating coil fluxmeter motor

E. Counter tube pumpout

F. Housing for counter high voltage terminal

G. Sample holder ring

H. Magnet coil and spool

J. Brass vacuum wall

P. Diffusion pump manifold

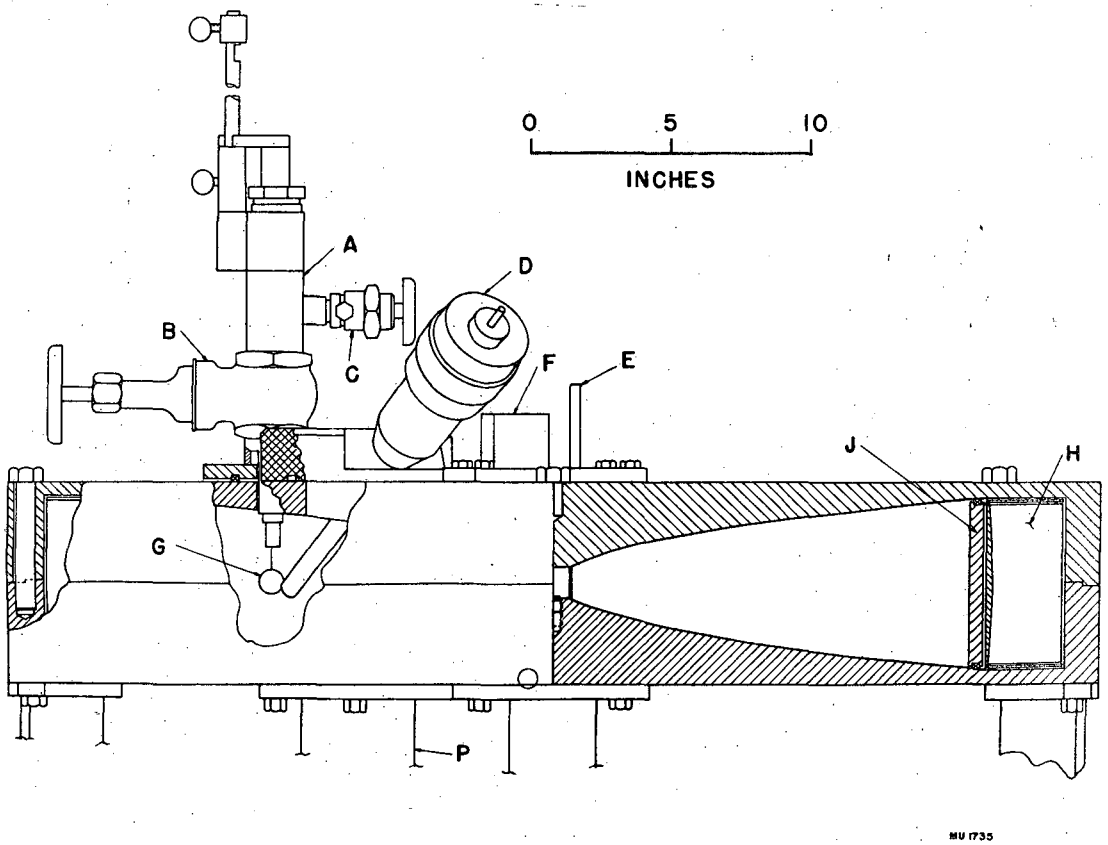
0
5
10
INCHES
A
B
C
D
E
F
G
H
J
P
MU 1735

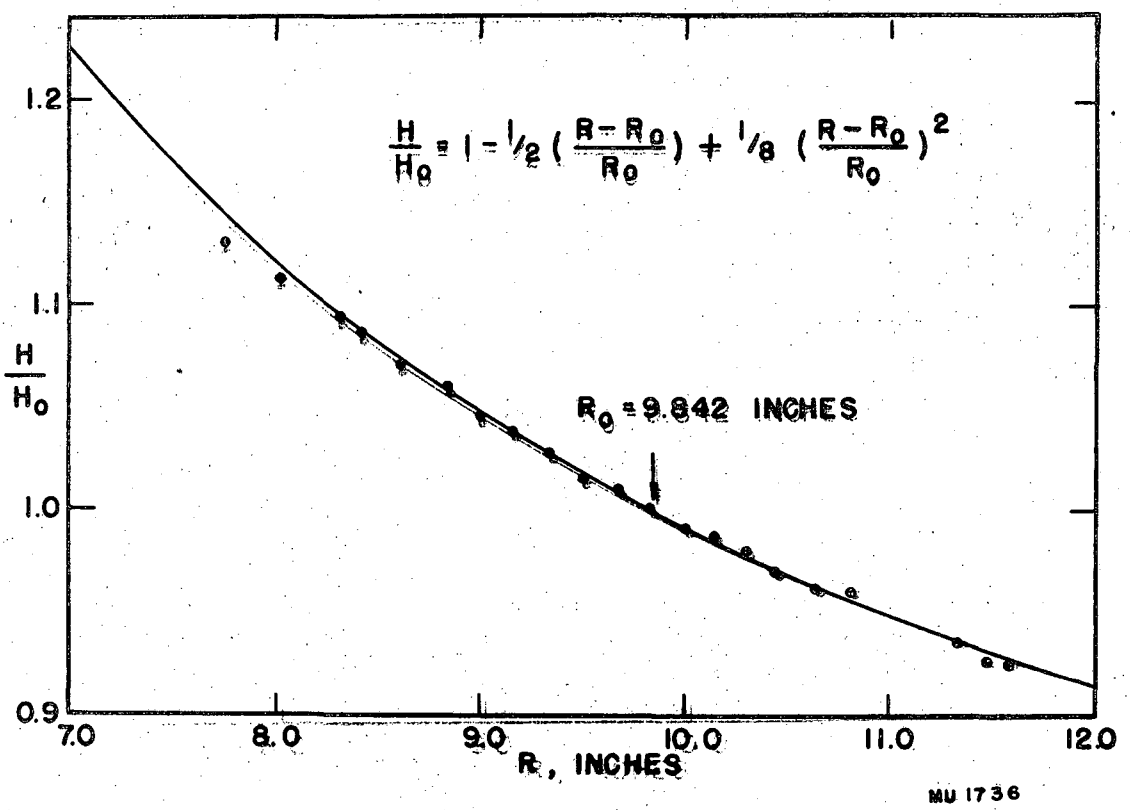

Fig. 6

Comparison of experimental and calculated field profile

applied to the rectifier is varied over a wide range. Two different control voltages are applied to the 304 - TL control tubes. The first is a variable bias, derived from a very stable 600 volt DC power supply; since the bias determines the plate current of the control tubes, the output current to the magnet coil can be adjusted in this way. A second control voltage is applied from a resistor in series with the magnet, which is sensitive to changes in magnet current which may occur, and transfers such changes to the control tubes as a correction signal. This system has the advantage of continuous current variation over the entire range of about 0 - 10 amperes with a single control. A simplified schematic diagram of the electronic circuit is shown in Figure 7.

In normal operation, the control bias is obtained through the "Remote Control" panel, which effectively divides the full current range into a series of 10 overlapping intervals and one coarse range of 0 - 10 amperes. The potentiometer on this unit can be driven by a motor of variable speed, and an auxiliary recording device indicates the magnet current as a function of time on a Leeds and Northrup multiple input "Speedomax" recorder which also plots the counting rate of the detector as a function of time. An exploratory sweep of a spectrum can thus be obtained quite conveniently, and this device has proved very useful.

For investigating low energy spectra, it is convenient to expand the low current ranges. This is achieved by switching a fixed resistor of approximately 0.1 the resistance of the magnet and its circuits across the output of the power supply, so while the power supply undergoes

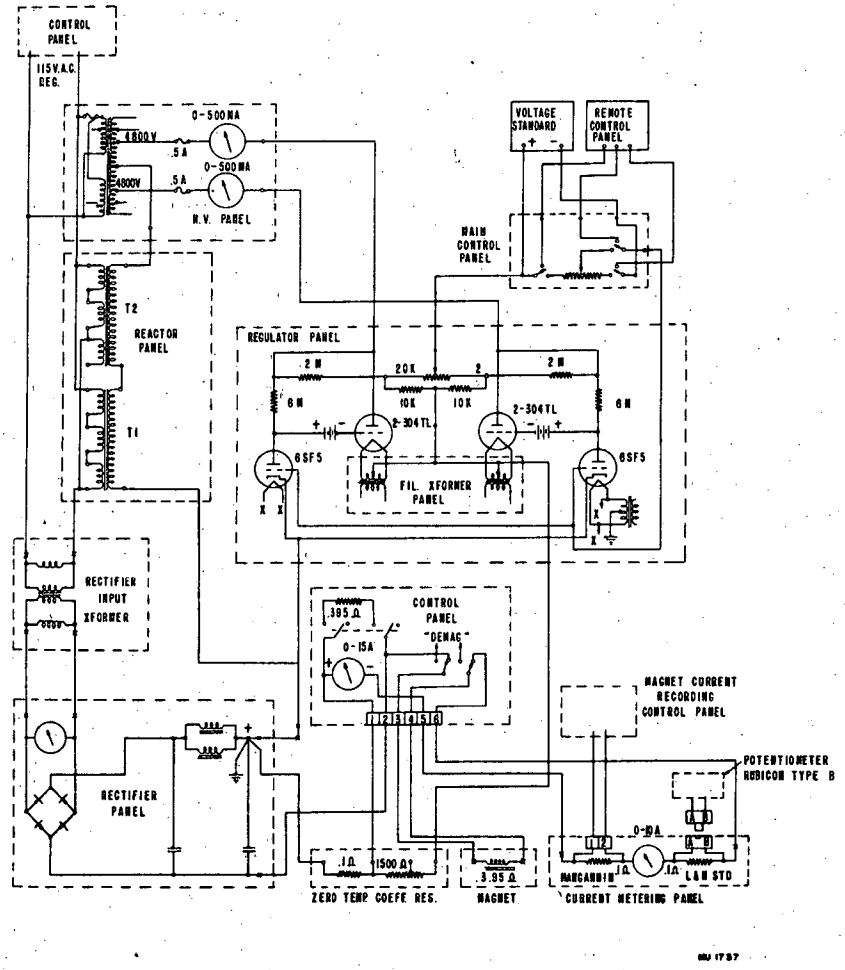

Fig. 7

Simplified schematic diagram of the magnet power supply

an excursion of 0 - 10 amperes in ten steps, the magnet current is about 0 - 1 ampere.

The current through the magnet coil is measured by observing on a null-type potentiometer the voltage drop across a 0.1000 ohm, 15 ampere Leeds and Northrup standard resistor.

Within the spectrometer are four polystyrene baffles, placed 15, 18, 21, and 237 degrees from the source. The baffles are fixed in aperture to allow a transmission of 1 percent of 4π for an inverse resolution of 1 1/3 percent. However, if the source has a large area, this high transmission cannot be attained; usually transmissions of 0.2 - 0.5 percent can be expected. With the slit apertures reduced, inverse resolutions of 0.36 percent have been used.

The pumping system consists of a Distillation Products Corporation VMF - 100 oil diffusion pump, backed by a Welch Model 1505-A Duoseal mechanical pump. The airlock through which samples are introduced is exhausted by a small, auxiliary mechanical pump. The diffusion pump oil is protected by safety devices which turn off the heating element if the cooling water fails or if the pressure in the vacuum tank exceeds about 30 microns of mercury pressure, as indicated on a National Research Corporation vacuum thermocouple.

With the pumping system described, a pressure of about 3×10^{-6} mm of mercury is obtained under operating conditions. Low Pressure measurements are made with a Western Electric D-79510 ion gauge, and a standard Radiation Laboratory ion gauge power supply described elsewhere.[37]

Detection is accomplished with a Geiger counter of the end window type, which is positioned at the focus of the spectrometer by an

adjustable brass support. This counter tube has a 1/4-inch brass collimator before the window, which is either a thin 0.0005-inch Nylon sheet or a Formvar foil 30-50 gm/cm^2 thick, supported on a Lectromesh grid. The windows are sealed with gaskets of dental dam rubber. Since such thin windows require that the tube be filled in situ, the counter tube is connected to an external evacuating and filling apparatus. Because of the solubility of the plastic windows in alcohol, ethylene is used as the quenching gas, the usual fill being 8.8 cm of a mixture of 10 percent ethylene and 90 percent argon.

To compensate for the loss of counter filling mixture by diffusion through the very thin windows a pressure regulating device has been installed, which operates as follows. When filled, the counter tube is connected to a 5-liter reservoir of filling gas at the operating pressure of 8.8 cm. Also attached to the counter tube is a mercury vacuum manometer with a wolfram contact just above the meniscus of the mercury column on the high pressure side. Should the pressure decrease, an electrical connection is made between the wolfram wire and the mercury column, which actuates a solenoid valve through a sensitive relay. This solenoid operated valve allows filling gas to be introduced from a high pressure reservoir until the counter system is again at 8.8 cm. A schematic layout of this regulator is shown in Figure 8.

The Geiger tube is connected to a quenching preamplifier of low deadtime, the output of which is fed to a standard scaler. In addition to the scaler, a counting rate meter of both linear and logarithmic response is used for making exploratory sweeps with the motor drive

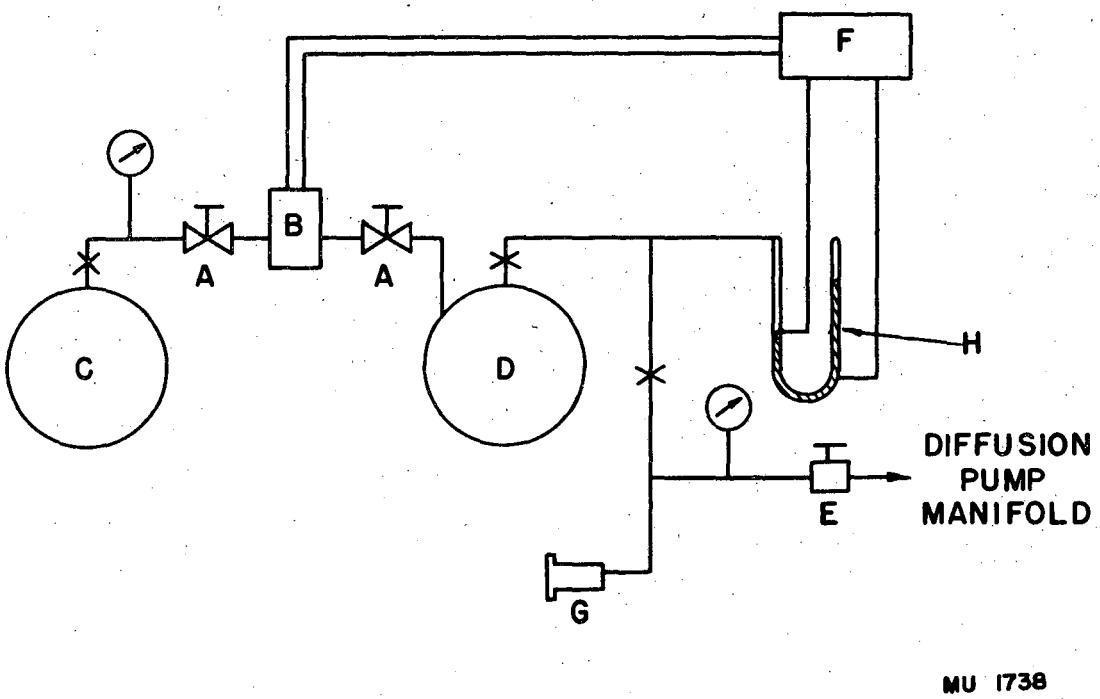

Fig. 8

Schematic diagram of counter tube pressure stabilizer

A. Sylphon type needle valves
B. Solenoid valve
C. 5-liter high pressure reservoir
D. 5-liter reservoir at 8.8 cm pressure
E. Counter tube pumpout valve
F. Electric circuit for actuating solenoid
G. Counter tube
H. Vacuum manometer, with electrical contacts which close with a decrease in pressure

unit of the magnet supply.

No departure from linearity between the magnet coil current and H has been observed either from direct field measurements or by measuring the current required to focus various monoenergetic conversion lines. However, there is some residual field which cannot be entirely eliminated, so the calibration equation has the form

$$H\rho = KI + c,$$

where K and c are evaluated by measuring the magnet current required to focus certain standard electron lines. The residual field contribution c is kept constant by passing zero to 1.5 amperes of alternating current through the magnet coil in a demagnetizing cycle, after which the direct current is always increased to avoid hysteresis effects. Figures 9 and 10 show curves of relative field as a function of magnet current, and $H\rho$ of some standard electron lines against magnet current, respectively.

Although the spectrometer was designed for a transmission of 1 percent for a resolution of 1 1/3 percent, the usual transmission is much lower, due to sample preparation, window absorption, and possibly other factors. The transmission at low energies is especially poor, since the supporting grid for the thin Formvar window is only 50 to 60 percent transparent. Above 200 Kev, where the 0.0005-inch Nylon windows can be used, the transmission is about 0.5 percent for a resolving power of 1.5 percent. However, in cases where a low transmission can be tolerated, very good resolving power can be obtained by decreasing the axial slit width and using carefully prepared sources. Some results for various Cs^{137} samples are shown in Figure 11.

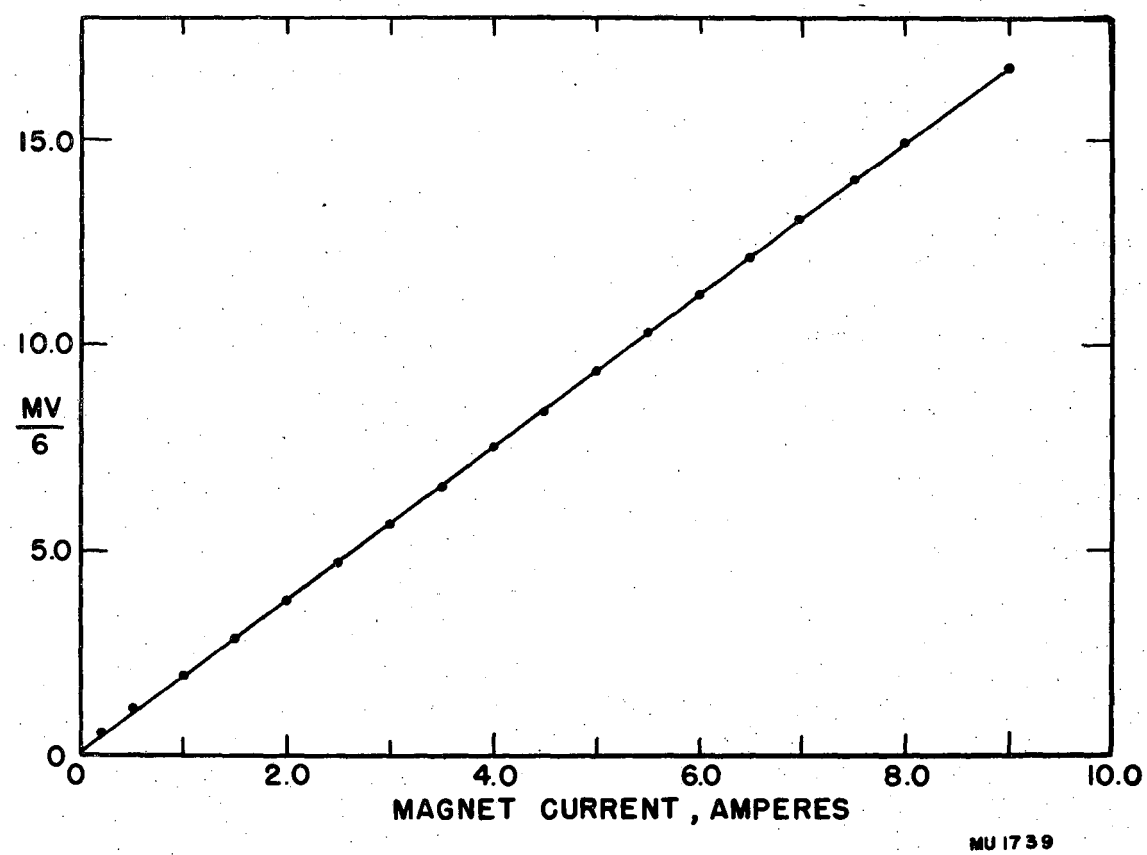

Fig. 9

Fluxmeter reading as a function of magnet current

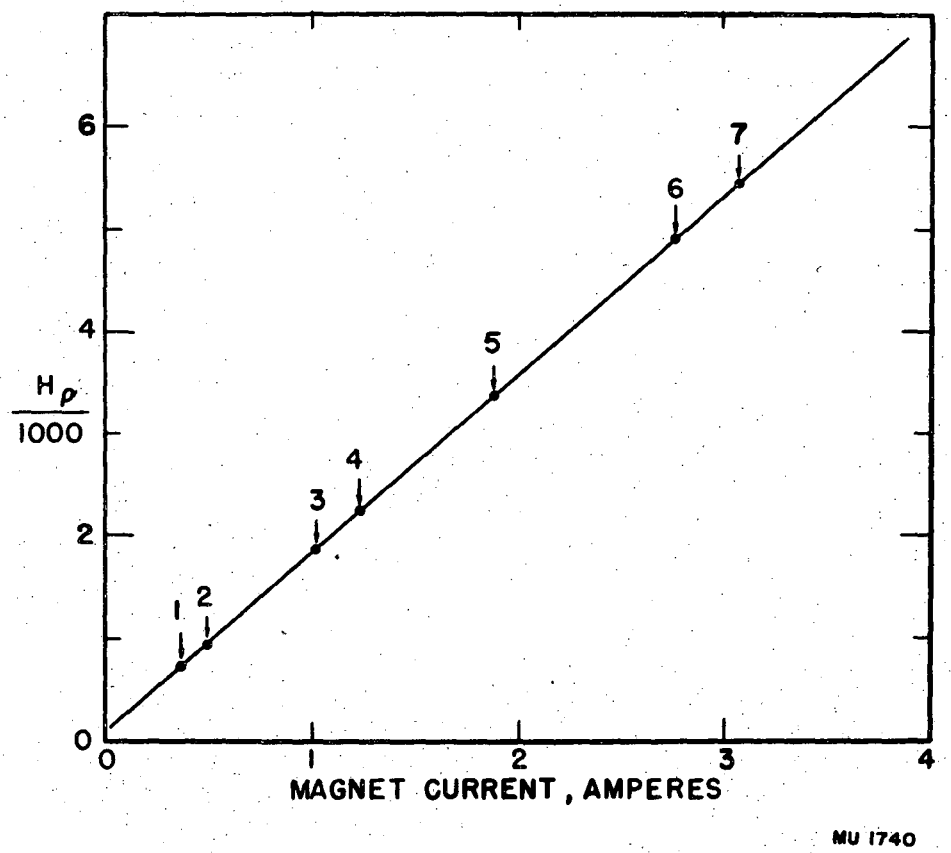

Fig. 10

Typical beta spectrometer calibration curve

1. K line of 0.08013 Mev gamma ray of I^{131}
2. L line of 0.08013 Mev gamma ray of I^{131}
3. K line of 0.2841 Mev gamma ray of I^{131}
4. K line of 0.3642 Mev gamma ray of I^{131}
5. K line of 0.6614 Mev gamma ray of Cs^{137}
6. K photoline of 1/172 Mev gamma ray of Co^{60} (uranium radiator)
7. K photoline of 1.332 Mev gamma ray of Co^{60} (uranium radiator)

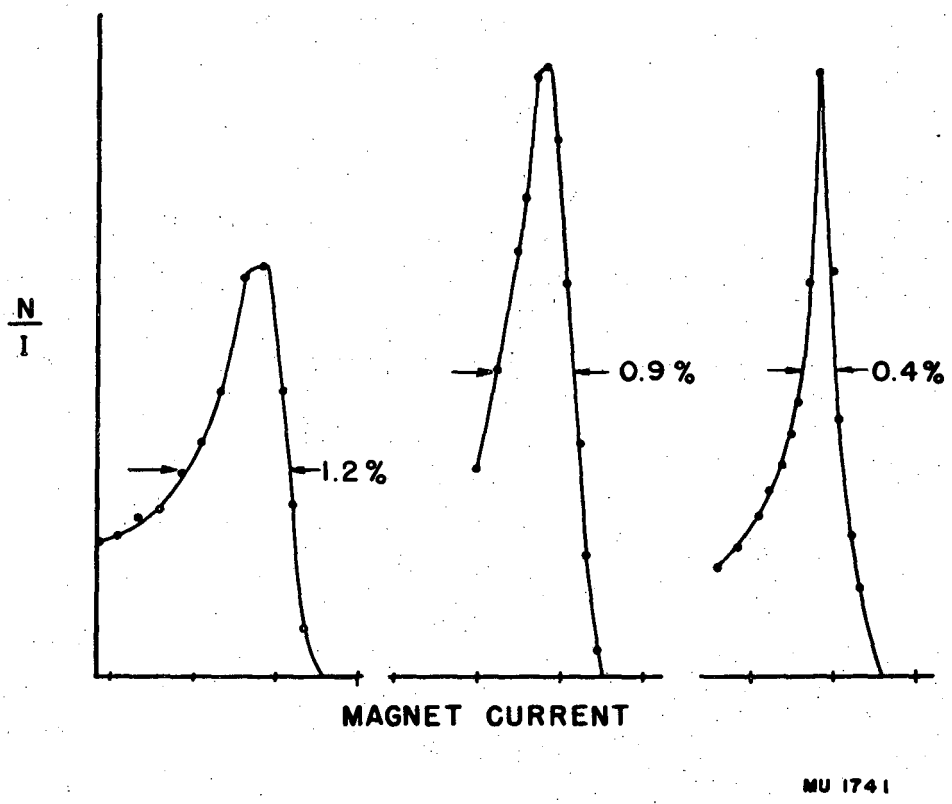

Fig. 11

The K internal conversion line of the Cs^{137} gamma ray, for three different samples and inverse resolution values.

Photographs of the magnet rack and the electronic equipment are shown in Figures 12 and 13.

III. EXPERIMENTAL

The beta spectrometer described above has been in routine use for about a year, and has been employed in a variety of investigations. The purpose of this section is to describe the author's research with this instrument.

Samples are generally mounted on thin Tygon plastic films 20-30 μgm/cm^2 thick which are coated with a thin layer of gold or aluminum evaporated in vacuum. Tygon is preferred over other plastics for such applications because of its acid resistance, as is the gold coating. The purpose of the metallic film is to ground the source to the source holder frame, which in turn is grounded to the spectrometer proper. If this grounding of the sample is not observed, serious shifts in low energy electron lines will result, particularly in samples which are extremely alpha radioactive.

Heavy alpha emitters consitute a great health hazard in the quantities employed for the investigations below. Indeed, the handling of large samples of transuranium elements requires considerably more care than the usual beta or gamma active samples encountered in beta spectroscopy, and contamination of the surroundings must be studiously avoided. In order to confine the alpha contamination in a small area, a glove box of transparent plastic was constructed by the Health Chemistry group of this laboratory, and is used for mounting the radioactive samples on the source probe. The probe is

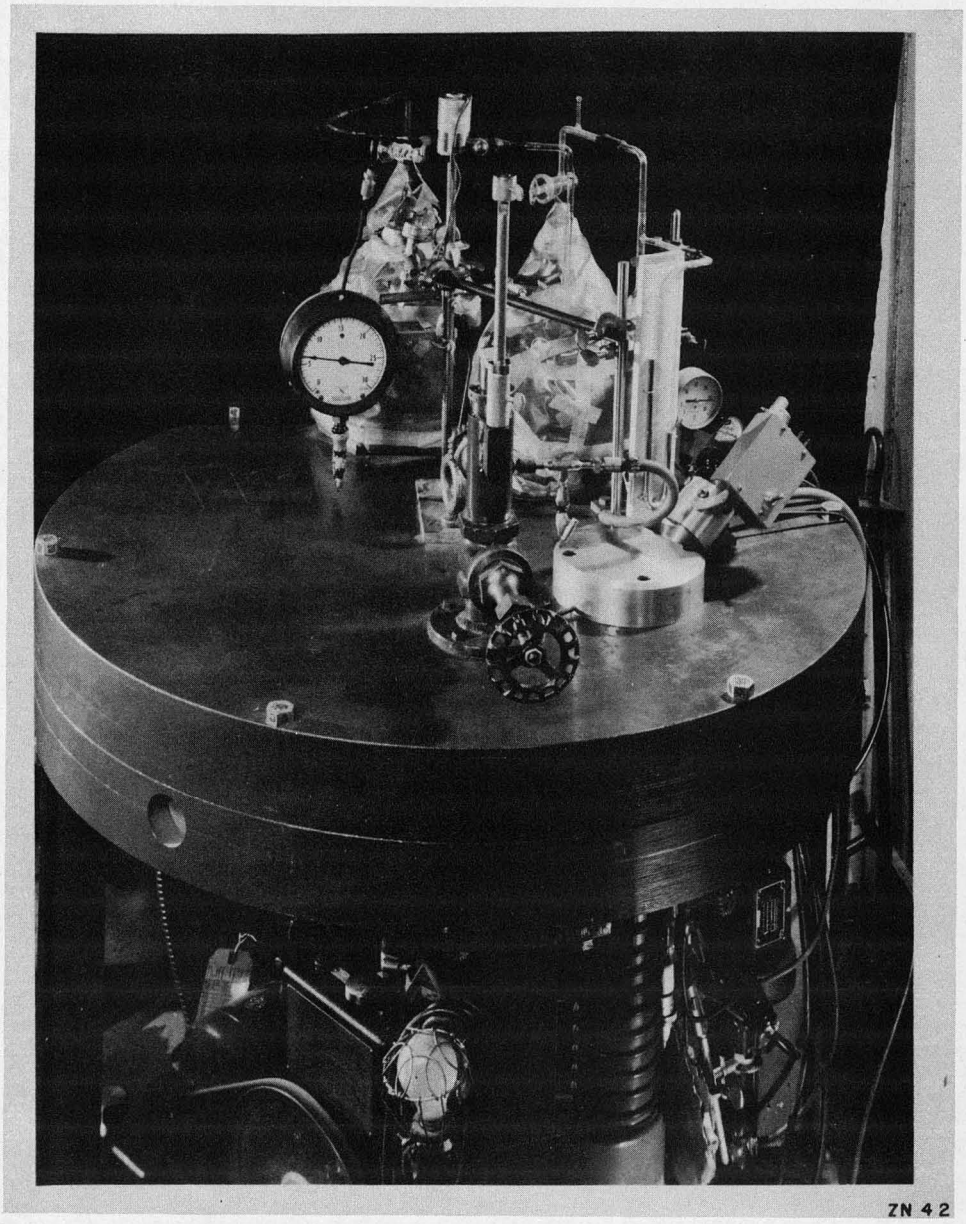

Fig. 12

Photograph of the beta spectrometer magnet rack

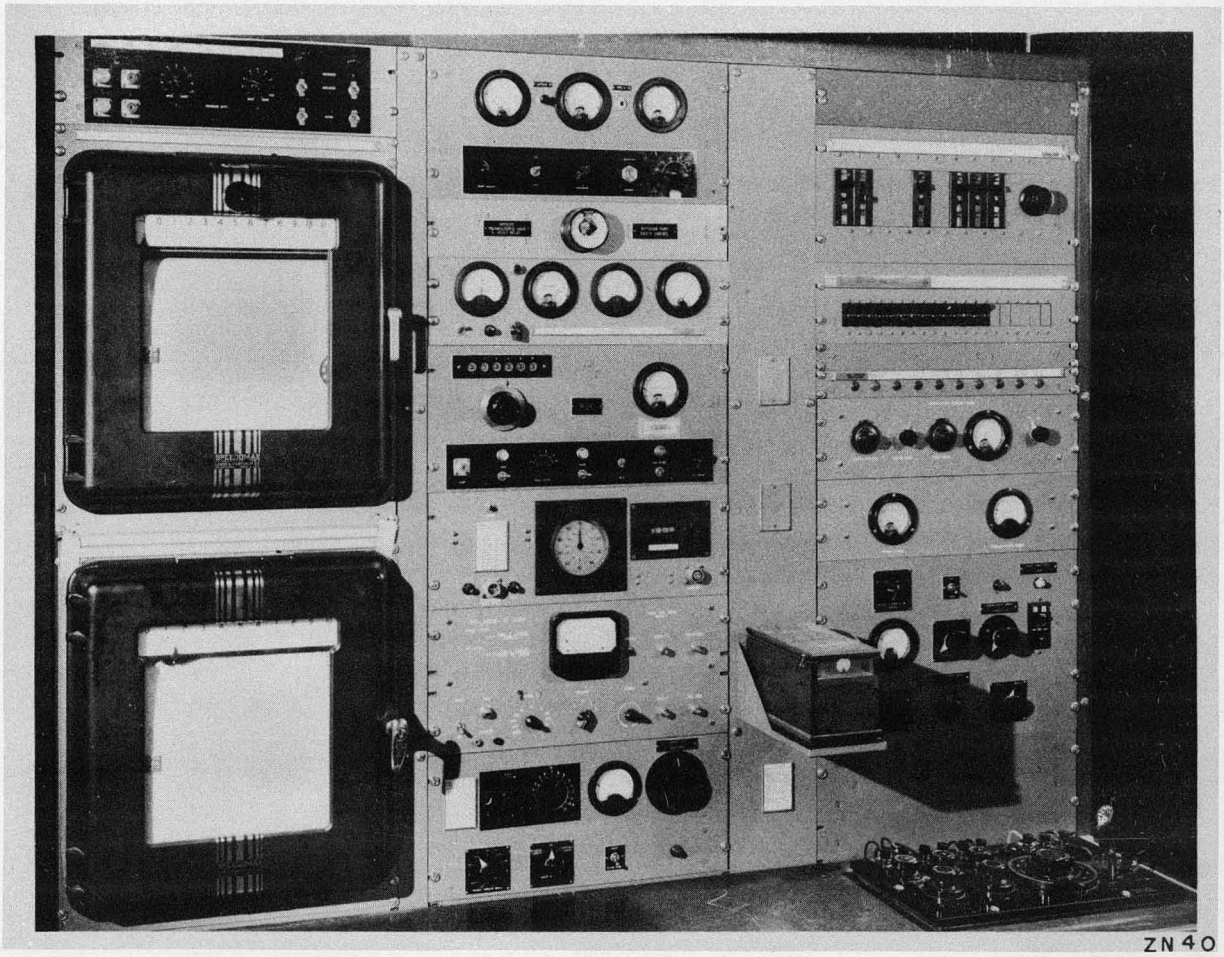

Fig. 13

Photograph of the auxiliary and control equipment for the beta spectrometer

introduced into the box through a Wilson seal, and after mounting the sample it can be inserted in the spectrometer airlock with a minimum possibility of contamination. A photograph of the glove box with a source in place is shown in Figure 14.

A. The Decay Scheme of Am^{242}

Neutron irradiation of 475 year Am^{241} results in the production of a pair of isomers[38,39] Am^{242m} with a 16 hour half-life known to decay by beta particle emission, and a long lived (100 year) ground state, Am^{242}, which is also a beta emitter and has weak alpha branching. Since strong sources of Am^{242m} and Am^{242} can be prepared by pile neutron irradiation of Am^{241}, it was possible to examine the radiations of the two isomers of Am^{242}, particularly Am^{242m}, with x-ray and beta spectrometers. As a result of these investigations, it became possible to characterize not only the beta transitions, but also the isomeric transition and electron capture decay.

The electron capture has been shown independently to result in the long lived nuclide Pu^{242} by mass spectrographic examination of the plutonium fraction from a sample of americium which had been subjected to long neutron irradiation.[40]

A curved crystal x-ray spectrometer proved very useful in analyzing the L x-ray mixture. This instrument and some of the other measurements for which it has been employed, have been described elsewhere by Barton, Robinson, and Perlman.[41] The x-ray spectrometer sample consisted of 2 mg of Am^{241} which had been irradiated with pile neutrons and repurified chemically. The pure americium was then

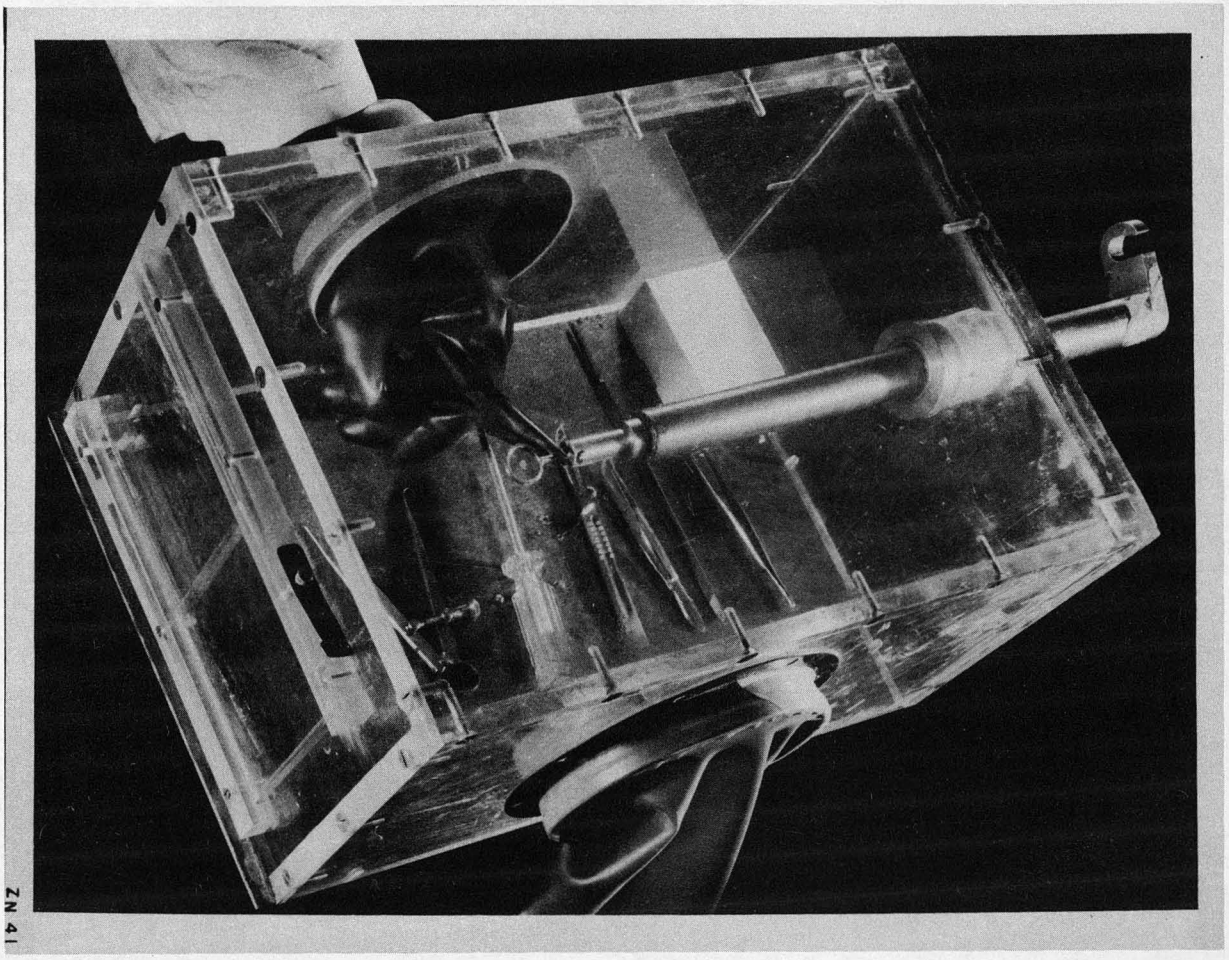

Fig. 14

Photograph of source probe glove box, showing source and probe in place

precipitated as AmF_3 and dried to a powder which was sealed in a thin walled, narrow glass capillary. This source gave very sharp peaks which allowed good energy measurements in the spectrometer. The spectrum was scanned with a motor sweep of constant speed, and the impulses from the scaler were recorded on a Streeter-Amet Trafi-counter. Approximately 6 hours were required to scan the L x-ray region; the decay of the lines was followed by scanning continuously for about six days. Figure 15 shows the decay over the 6 day period.

The L series x-rays of curium, americium, plutonium, and neptunium were positively identified from the close agreement with the values calculated by Barton using the Moseley relation. The validity of this extrapolation of x-ray energies into the transuranium region has been established by the work of Barton[41] on the L x-rays of plutonium and neptunium. The curium, americium, and plutonium x-rays were observed to decay with a half-life of about 16 hours, while the neptunium x-rays did not decay appreciably over the 6 day period. Presumably the origin of the x-rays is as follows: the curium x-rays arise from the internal conversion of a gamma ray following the beta transition, those of americium are from the internal conversion of the isomeric transition gamma ray, and the plutonium x-rays most probably arise from a combination of L electron capture and internal conversion processes. The long lived neptunium x-rays are to be expected from the internal conversion of the gamma ray of Np^{237} following the alpha decay of the target material, Am^{241} (see Section B).

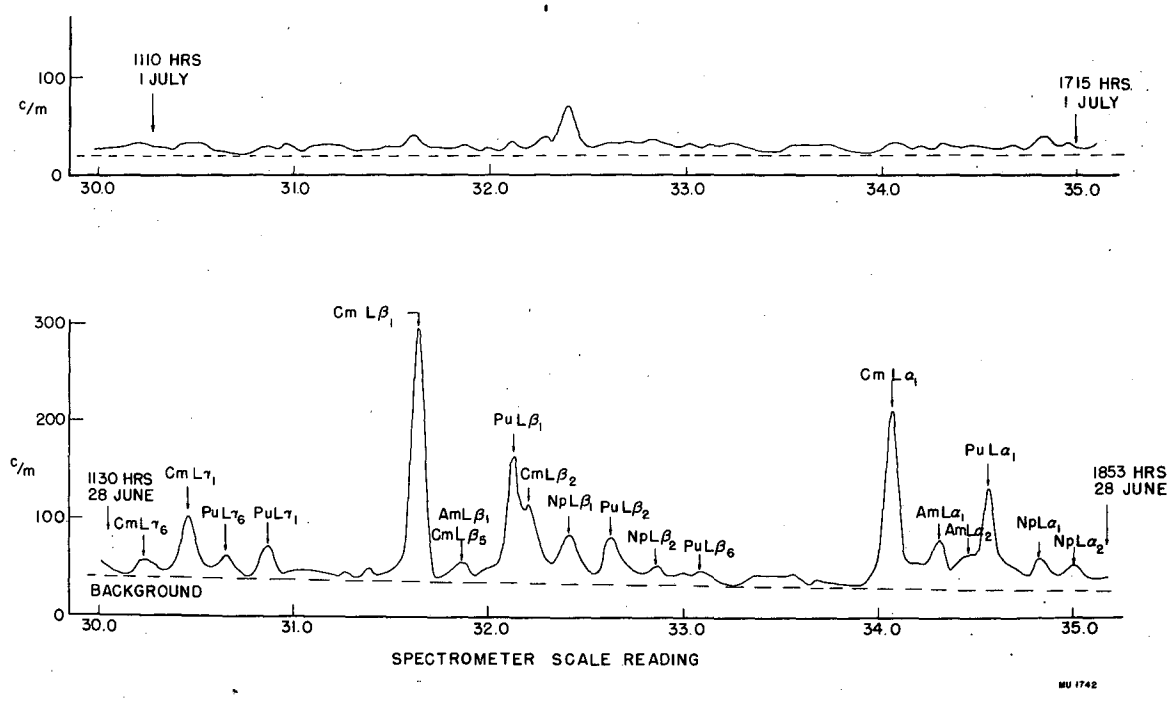

Fig. 15

L x-rays from decay of Am^{242m}, showing decay of lines

The relative intensities of the x-rays of curium, americium, and plutonium are of great importance to the formulation of a decay scheme. The observed intensities were corrected for absorption in the source capillary, quartz diffracting crystal, and counter window by assuming these effects to be equivalent to 150 mg/cm^2 of aluminum, and using Allen's compilation of absorption coefficients.[42] The xenon filled proportional counter efficiency for the various x-ray energies was estimated from the work of Crane and Ghiorso,[43] while the reflectivity of the quartz crystal was assumed to vary as $1/E^2$, as calculated by Lind, West, and Dumond.[44] Barton, Robinson, and Perlman have found that the relative intensities of the x-rays involving the L_{III} level ($L\alpha_1$, $L\beta_2$, etc.) agree well with those of electron bombarded uranium.[41] The intensities of the x-rays from the decay of Am^{242m} were normalized, taking the relative intensity of the curium $L\alpha_1$ line as 100. Here also, there is agreement between intensities from excitation of uranium by electron bombardment and excitation by the internal conversion process and electron capture in the cases of the $L\alpha_1$ and $L\beta_2$ lines. However, it is also interesting to note that the x-rays involving the L_{II} and L_{III} levels are in approximately equal abundance for the plutonium and curium x-rays, but the americium L_{III} x-rays from the isomeric transition are about five times as abundant as the L_{II} level radiation. Selection rules are probably in force such that the L_{III} level is especially favored, and may well be related to the long life of the isomeric state. This unusually large number of L_{III} transitions is noticeable in the conversion electron spectrum, and is in disagreement with Kinsey's assumption[45]

that the L_I level is always the most strongly excited in the internal conversion process, although in the cases of curium and plutonium x-rays the ratio of L_{II} x-rays to L_{III} x-rays is about that reported by Kinsey. Table 1 lists the principal lines observed, their measured energies and intensities.

Table 1

Principal x-ray lines in decay of Am^{242m}

X-ray line designation		Level transition	Measured energy	Relative intensity (corrected)[a]	Calculated energy
Pu	$L\alpha_1$	$L_{III} - M_V$	14.33 ± 0.01	68	14.31
	$L\beta_2$	$L_{III} - N_{IV}$	17.32 ± 0.02	22	17.29
	$L\beta_1$	$L_{II} - M_{IV}$	18.34 ± 0.02	54	18.30
	$L\gamma_1$	$L_{II} - N_{IV}$	21.52 ± 0.05	18	21.43
Am	$L\alpha_1$		14.66 ± 0.02	39	14.66
	$L\beta_2$		[b]		
	$L\beta_1$		18.90 ± 0.07	8	18.84
	$L\gamma_1$		[b]		
Cm	$L\alpha_1$		15.01 ± 0.01	100	15.00
	$L\beta_2$		18.13 ± 0.04	36	18.08
	$L\beta_1$		19.48 ± 0.02	107	19.38
	$L\gamma_1$		22.78 ± 0.07	33	22.68

[a]Estimated corrections for crystal and counter window absorption and reflection intensity variation with energy.

[b]Not resolvable from other lines.

Microgram quantities of purified, neutron irradiated americium were used for preparing the beta spectrometer sources. Conducting Tygon films were used as backings. In the course of the investigation, six different samples were observed and four pile irradiations of Am^{241} were made.

The beta spectrum of Am^{242m} was determined on each of the four bombardments and Fermi-Kurie plots of the data were made. Calibration in this energy region was made against the K electron line of the Cs^{137} gamma ray, whose magnetic rigidity of 3381 gauss-cm has been precisely compared with the K line of the 0.4112 Mev gamma ray of Au^{198} by Langer.[46] Figure 16 shows a typical Fermi-Kurie plot. Table 2 lists the values of the beta energy obtained, from which the final value of 628 Kev is obtained, and the absolute uncertainty is estimated to be $\pm$ 5 Kev.

Table 2

Determinations of Am^{242m} beta energy

Experiment	Beta energy, Kev
1	628
2	628
3	625
4	630

There is some evidence that the beta spectrum of Am^{242m} is complex, with a second component at about 280 Kev. At the present writing, evidence for a 350 Kev gamma ray is not definitive, due to the possibility of a small amount of fission product activity which may have followed the chemical separations. Attempts to precisely measure the beta energy of the 100 year Am^{242} isomer failed because of insufficient activity, using the above samples. However, Dr. S. G. Thompson kindly

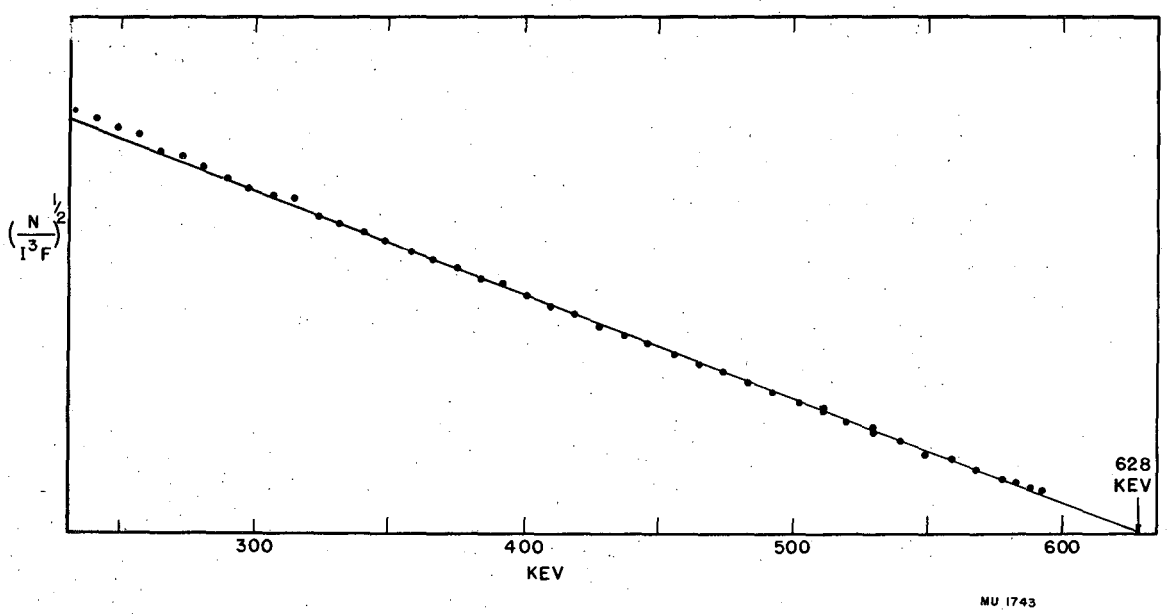

Fig. 16

Fermi-Kurie plot of Am^{242m} beta spectrum

prepared a sample of $Am^{241,242}$ with fairly high specific activity of Am^{242}. From this source, a value of 593 Kev for the beta energy of the long lived isomer was obtained.

Lead and copper absorption curves of the electromagnetic radiation from the 16 hour isomer showed only a soft gamma ray of about 50 Kev and L x-rays, but no detectable hard gamma radiation or K x-rays.

A portion of the low energy electron spectrum in which lines were seen is shown in Figure 17. The resolving power of the spectrometer was adjusted to about 0.5 percent, but at the low energies encountered in these experiments, backscattering from the sample backing introduces a smearing effect which is very difficult to eliminate. The electron lines have not been corrected for window absorption in Figure 17, but estimates of relative abundances were made, using window absorption corrections published by Heller, Strucker, and Weber.[47]

The electron lines are assigned to the L internal conversion of gamma rays of 53 Kev, 35 Kev, and 38 Kev, assuming these gamma rays to result from transitions in curium, americium, and plutonium, respectively. These assignments are based on the energy differences of the lines, which seem to best match the L_I, L_{II}, and L_{III} differences of curium, americium, and plutonium. Such assignments are not conclusive, since the experimental uncertainties are of about the same order as the differences. However, further evidence is obtained from the decay of the lines. It is observed that the electron lines of the 35 Kev gamma ray decay with a half-life of 15 to 20 hours, while the lines of the 53 and 38 Kev gamma rays decay initially with a short half-life of this order, but gradually tail into a half-life which is

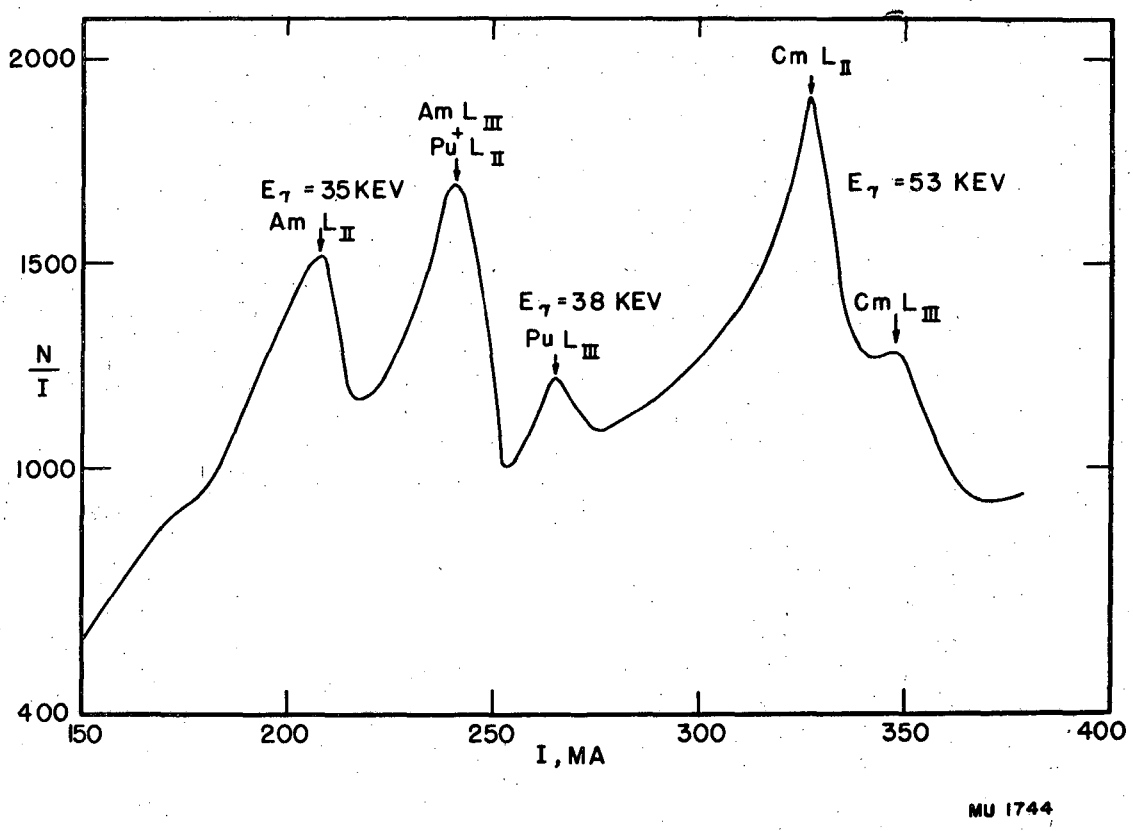

Fig. 17

Low energy electron lines of Am^{242m}

very long. It seems reasonable that the 53 Kev gamma ray should be associated with the beta transition, since this is the predominant decay process, and the 53 Kev gamma ray is seen in absorption measurements. The 53 Kev gamma ray is approximately 40 percent converted, if it follows the beta decay. This is to be compared with a value of 50 percent, based on absorption measurement by Crane.[48]

On the assumption that the 53 Kev gamma ray is 40 percent converted, that the other two gamma rays are 20 percent converted, and that the L Auger coefficient is about 0.5, the relative probabilities for the various decay processes can be estimated. Am^{242m} appears to decay 15 percent by electron capture, 15 percent by isomeric transition, and about 70 percent by beta emission.

Since the 38 and 53 Kev gamma rays were observed to be present in both 16 hour Am^{242m} and 80 year Am^{242}, it is assumed that the beta decay of the long lived isomer excites the same 53 Kev level in Cm^{242} as the 16 hour activity, and that the electron capture involves a transition to the level in plutonium 38 Kev above the ground state. Evidence with the one sample of pure 80 year Am^{242} investigated thus far indicates that such is the case, although there is some preliminary evidence for a harder gamma ray also following the electron capture.

The experimental results discussed here can be summarized as a decay scheme, which is shown in Figure 18.

B. Radiations of Am^{241}

Since 475 year Am^{241} is produced in milligram quantities in nuclear reactors, its chemical properties have been extensively

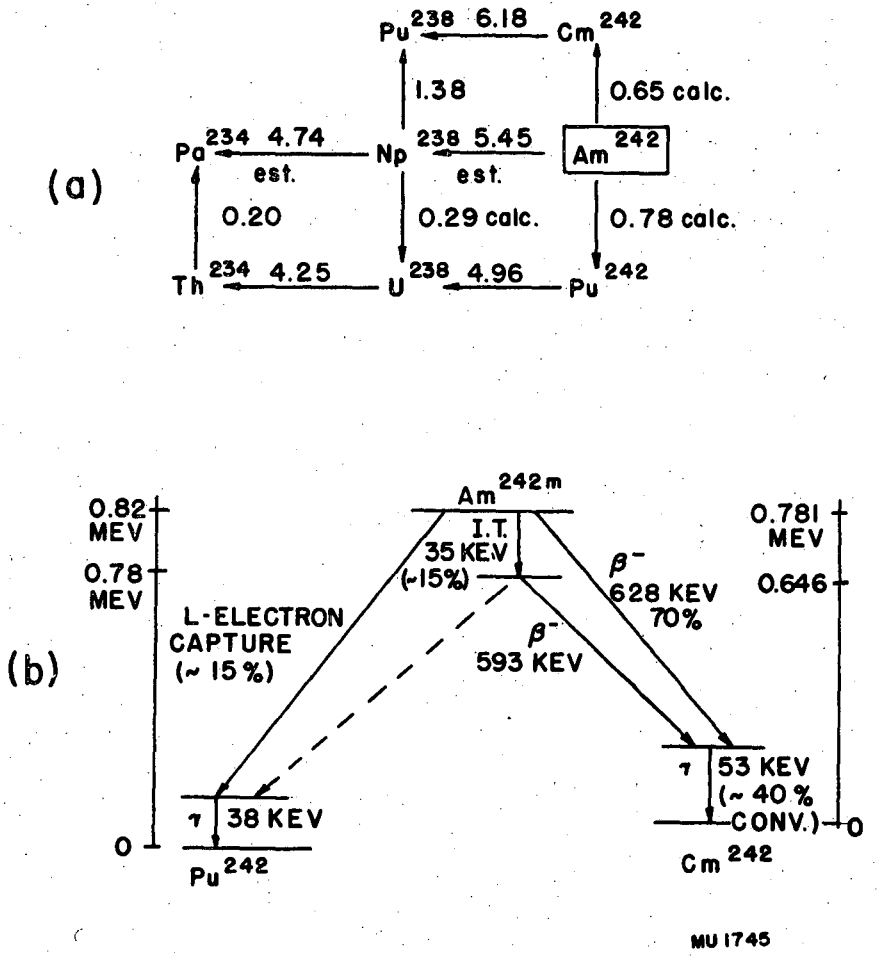

Fig. 18

Proposed decay scheme of Am^{242}

studied in this laboratory, using weighable quantities of material. Because of its availability and possible use as a counting standard, this nuclide was investigated on the beta ray spectrometer.

Seaborg and co-workers[38] had found that the nuclide Am^{241} emits gamma rays of about 62 Kev, and in an intensity of about 0.4 per alpha particle. These workers also found x-rays of about 20 Kev, which were the L x-rays of neptunium. Barton, Robinson, and Perlman[41] measured these x-rays on the x-ray spectrometer and showed that they indeed arose from transitions in neptunium. (See also Section A above.)

The samples of Am^{241} were mounted as previously described, using thin backings, but macro amounts of material. Both Auger electrons from L type transitions and internal conversion electrons were observed. The L, M, and N conversion lines of a 59.4 ± 1.0 Kev gamma ray are shown in Figure 19. This gamma ray energy checks the absorption value quite closely.

The internal conversion coefficient of this gamma ray can be estimated from the electron line intensities. Obtaining the transmission of the spectrometer as described in Section C below, the ratio of L electrons to total alpha particles was found to be 0.28. Since the abundances of the two alpha particle groups are not known accurately, it was necessary to calculate the internal conversion coefficient from the ratio of gamma rays to alpha particles, which was taken as 0.4. Thus it appears that this gamma ray is about 40 percent L converted, i.e., $\alpha_L \simeq 0.7$. One may also estimate from these data that about 70 percent of the Am^{241} alpha transitions excite a level in Np^{237} 59 Kev above the ground state, and that the remaining 30 percent of

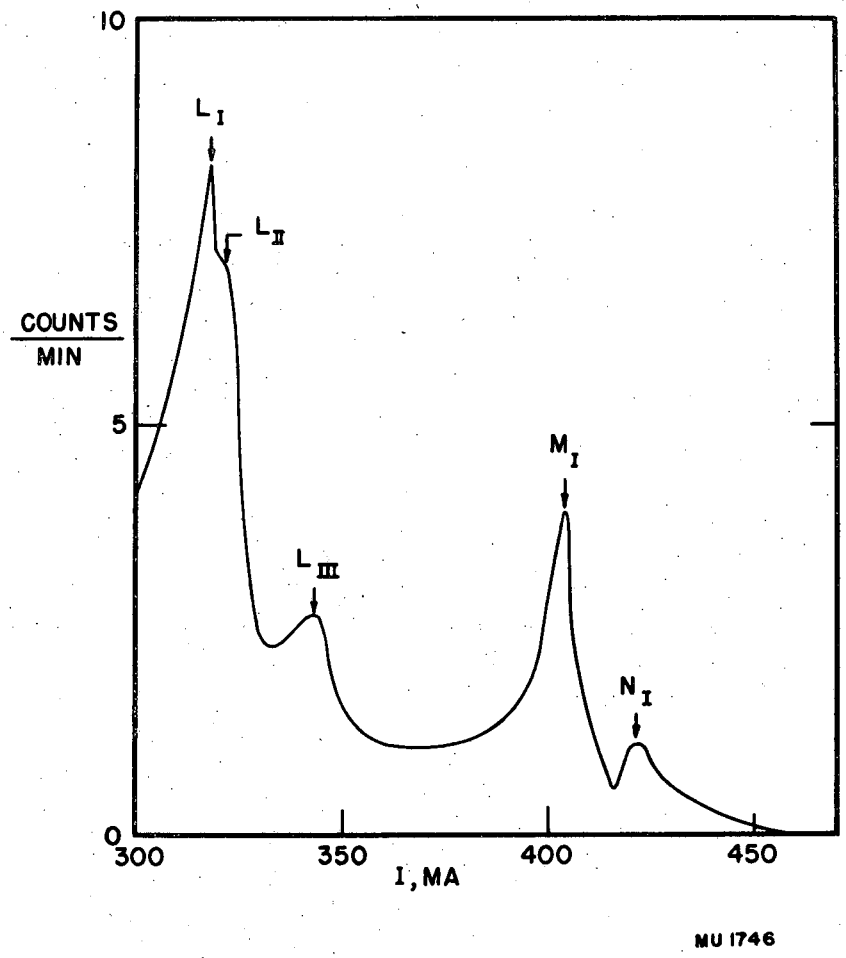

Fig. 19

Electron spectrum of Am^{241}

the alpha transitions are to the ground state of Np^{237}. These estimates of abundances are probably accurate to ± 20 percent. The postulated decay scheme is included in Figure 19.

C. Decay Scheme of Cm^{242}

The nuclide Cm^{242}, an alpha particle emitter of 163 days half-life, can be prepared in microgram quantities by neutron irradiation of Am^{241}, and the subsequent decay of Am^{242m} as described in Section A, above. Absorption experiments indicate L x-rays and a gamma ray of about 50 Kev. No hard electromagnetic radiation is detectable.

Intense Cm^{242} sources were obtained from W. W. T. Crane and run on the beta spectrometer, with the result that Auger electrons and internal conversion electrons were observed (Figure 20). The internal conversion lines can be assigned to the L, M and perhaps the N conversions of a 43 Kev gamma ray. From measurements of the line intensities, it is possible to estimate the conversion coefficient. With this in mind, the geometry and detector efficiency of the spectrometer were measured by extrapolating a Fermi-Kurie plot of a sample of Pm^{147} to low energies, and correcting the low energy points up to the straight line. The spectrum of Pm^{147} is known to follow the allowed shape down to about 8 Kev,[49] so such a procedure is valid of scattering effects are not too severe. The sample of Pm^{147} was about the same size and weight as the Cm^{242} source, in order that the "luminosities" would be the same. A further datum required is the relative abundances of the two alpha groups. Asaro and Perlman[50] have found the high energy alpha group to be in 70 percent abundance, while the other, which

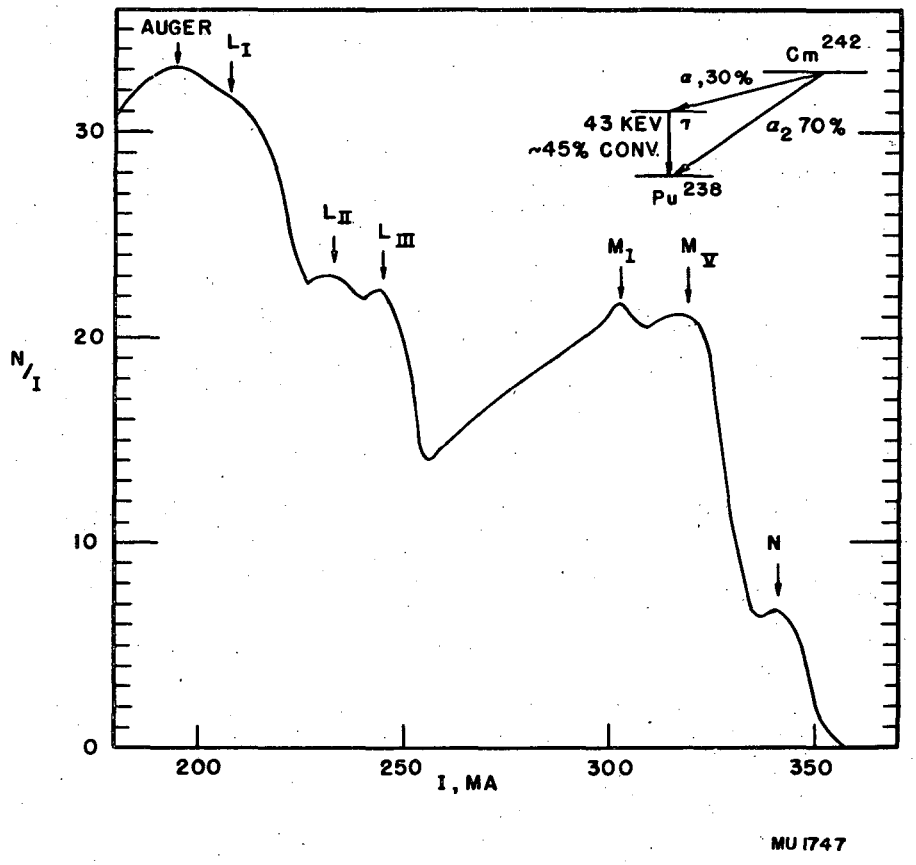

Fig. 20

Electron spectrum and decay scheme of Cm^{242}

precedes the 43 Kev gamma ray, is present in 30 percent abundance. The conversion coefficient is calculated as follows:

$$\text{conversion coefficient} = \frac{\text{(Total electrons detected)}}{0.3\ \text{(Transmission)(total alpha disintegrations)}}$$

For the L conversion electrons, this was measured as about 45 ± 10 percent. The ratio of L conversion to M conversion is about 5.

These data are consistent with the decay scheme shown on Figure 20.

D. Decay Scheme of 22 hour Np^{236} and 4.4 day Np^{234}

A consideration of the closed energy cycles relating to the decay of Np^{236} indicated (Figure 21-a) that electron capture was energetically possible to the extent of 1.21 Mev in addition to the beta emission already known to occur.[51] An investigation of this isotope was undertaken in the hope that both the beta decay and electron capture branching could be detected and the relative intensities measured.

The samples of Np^{236} were prepared by bombardment of U^{235} with 14 Mev deuterons from the 60 inch cyclotron at the Crocker Radiation Laboratory. Smaller amounts of Np^{234} were also produced in these bombardments. The target material was dissolved and a radiochemically pure neptunium fraction was separated by D. A. Orth. The final step of the chemical procedure was an elution of the neptunium fraction from an anion exchange column with concentrated HCl. Thus it became possible to prepare carrier free samples of neptunium of high specific activity. Beta spectrometer sources were mounted on thin Tygon plastic films about 20-30 gm/cm^2 thick. Tygon was very useful in this application, since a drop of concentrated HCl may be evaporated on such a film without mishap. As a precaution against source charging, a thin layer of gold

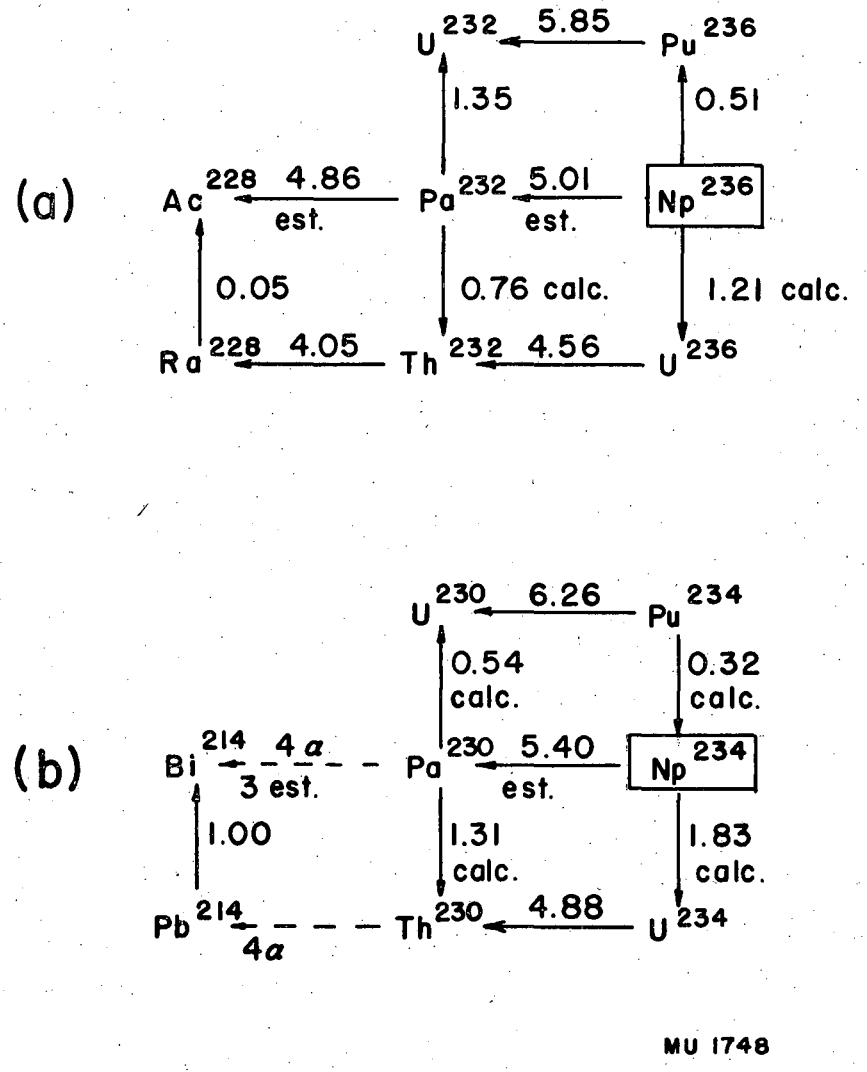

Fig. 21

Closed decay cycles involving Np^{236} and Np^{234}

was evaporated over the plastic film and the source holder ring, which was then grounded to the spectrometer frame.

When samples of Np^{236} were examined on the beta spectrometer, Auger electrons, internal conversion electrons, and beta particles were seen. Figure 22-A shows the electron spectrum obtained. The L Auger electrons are far too intense to be accounted for by the internal conversion of the gamma rays shown. Fermi-Kurie plots (Figure 22-B) of the continuous beta spectrum are complex, and two beta groups may be resolved, having energies of 0.51 Mev (59 percent) and 0.36 Mev (41 percent). A pair of internal conversion lines corresponding to the K and L conversion of a 0.150 Mev gamma ray was also observed. Assuming this gamma transition to follow the 0.36 Mev beta transition, the gamma ray is about 100 percent converted, with a ratio of K electrons to L electrons of about 22. A powerful argument in favor of this scheme is the calculated disintegration energy of 0.51 Mev from the closed energy cycles of Figure 21.

It was briefly mentioned that the Auger electrons observed were far in excess of those expected from K and L electron vacancies due to the internal conversion of the gamma rays, or from the electron capture in the Np^{234} which was also present. These electrons, when corrected for the presence of Np^{234}, are a measure of the electron capture in Np^{236}. However, window corrections for the beta spectrometer detector are uncertain in this low energy region, and so it was deemed desirable to use absorption methods to evaluate the relative number of electron capture and beta transitions. The radiations were resolved by beryllium and silver absorption into electrons, L x-rays,

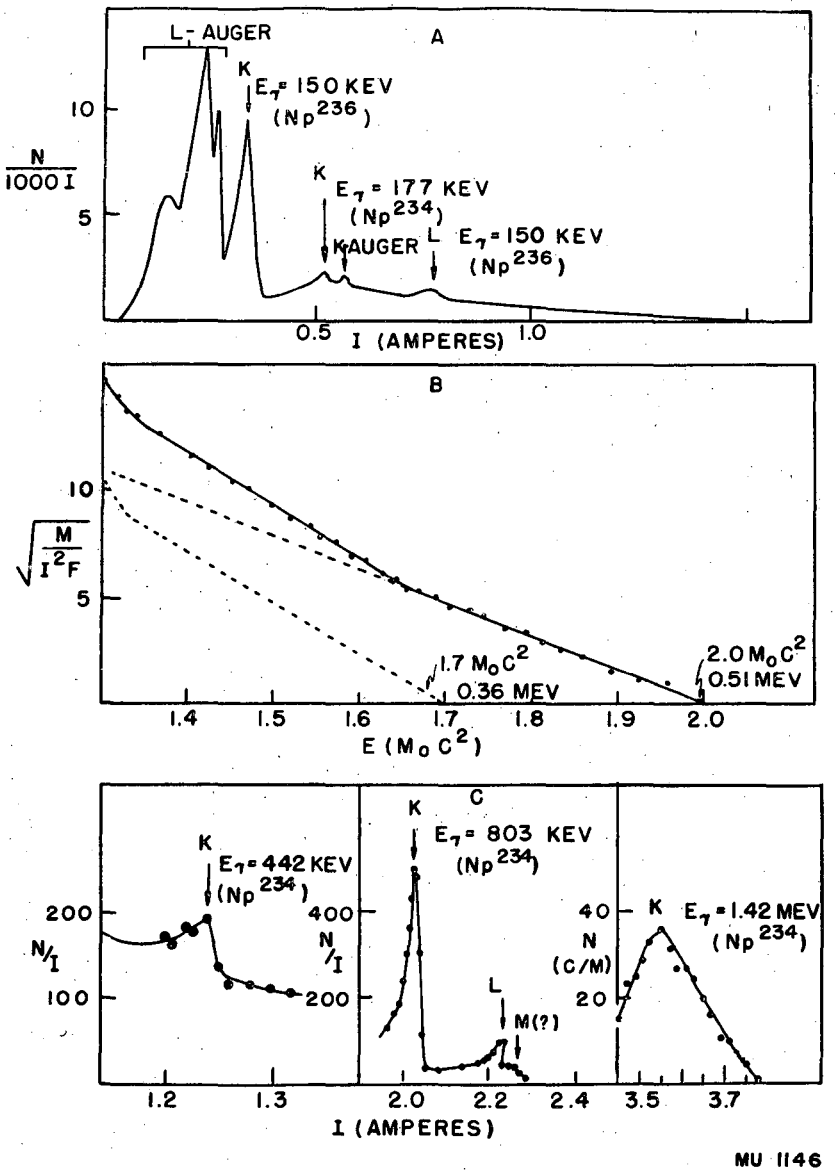

Fig. 22

A. Electron spectrum of Np^{236} and Np^{234}

B. Fermi-Kurie plot of Np^{236} beta spectrum

C. Additional electron lines from Np^{234}

and K x-rays, as described elsewhere.[52] The relative intensities were corrected for the counting efficiency of the detector and the L Auger coefficient, which was assumed to be 0.5 from the work of Kinsey.[45] An estimate of the K electron capture was made, taking into account the internal conversion of the 0.15 Mev gamma ray in the K shell. Further, the total L vacancies calculated from the absorption data minus the number of L vacancies resulting from the K vacancies is taken as the number of L electron capture vacancies. Relating these intensities to the number of beta particles allows the completion of the decay scheme, in which the relative abundances should be accurate to ± 20 percent (Figure 23-a).

Although there is a large amount of L electron capture for this disintegration energy of 1.21 Mev, other heavy nuclides such as U^{231}, Np^{235}, and Am^{242m} have demonstrated predominant capture of L electrons.[53,54,55]

Besides the conversion line of the 0.177 Mev gamma ray of 4.4 day Np^{234} shown in Figure 22-A, another group of rather prominent lines are found beyond the Np^{236} beta spectrum which correspond to the K, L, and possibly the M internal conversion of a 0.803 Mev gamma ray. These lines decay with a 4 day half-life, and thus are associated with the decay of Np^{234}. The closed decay cycle of Figure 21-b shows the electron capture energy of Np^{234} to be 1.87 Mev. There is also a line of low intensity at even higher energy, which has a longer half-life than Np^{236}, and is most probably the K internal conversion peak of a 1.42 Mev gamma ray. If a mixture of Np^{234} and Np^{236} is allowed to decay for several half-lives of the latter, it becomes possible to resolve out

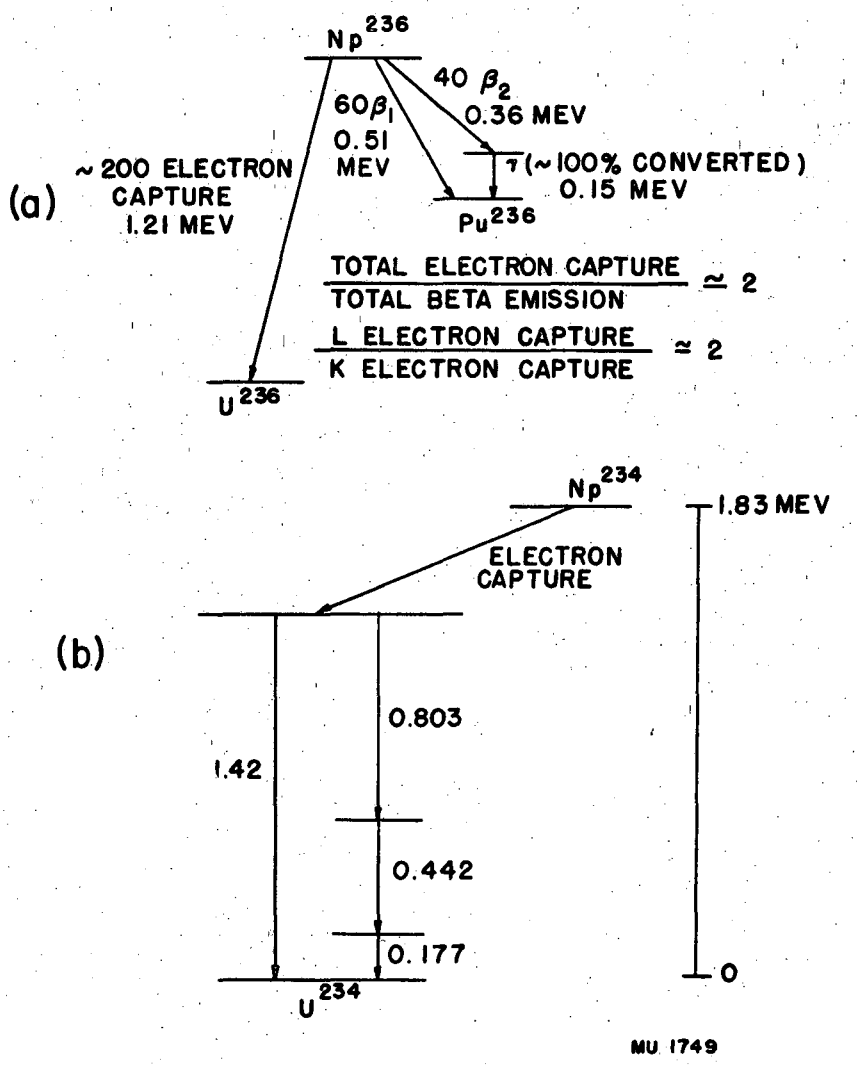

Fig. 23

Decay scheme of (a) Np^{236} and (b) Np^{234}

the K electron line of a 0.442 Mev gamma ray of Np^{234}. The electron spectrum of these gamma rays is shown in Figure 22-c. Although an extensive study of the decay scheme of Np^{234} has not been made, it seems apparent that this electron capture nuclide has associated with its decay gamma rays of 0.177 Mev, 0.442 Mev, 0.803 Mev, and 1.42 Mev. A rather straight forward interpretation of these data is that the first three gamma rays are in cascade, with the 1.42 Mev gamma ray a crossover transition. This scheme is shown in Figure 23-b.

It would be very interesting to examine the gamma ray spectrum of Np^{234} more thoroughly, and especially to obtain the relative gamma ray intensities.

E. Radiations of Pu^{243} and Pu^{238}

The electron capture in Am^{242m} has been shown[40] to result in the long lived plutonium isotope, Pu^{242}, while the beta decay of Am^{242m} forms Cm^{242}. If the plutonium fraction is separated from a sample of Am^{241} which has been subjected to long neutron irradiation, both Pu^{242} and Pu^{238} are present in about equal amounts by weight,[40] the latter plutonium isotope resulting from alpha decay of Cm^{242}. Alpha pulse analysis and mass spectrographic measurements of these plutonium samples showed the alpha particle energy of Pu^{242} to be 4.88 Mev and the alpha particle half-life to be approximately 5×10^5 years, in good agreement with the alpha decay systematics.[3,4] Energy surface considerations in this region indicate beta stability for both Pu^{242} and Pu^{238}. Recently the half-life of Pu^{238} has been measured as 89.59 ± 0.37 years,[56] and the alpha particle energy as 5.47 Mev.[57]

Neutron irradiation of Pu^{242} has been shown to result in the 5.0 ± 0.2 hour beta activity Pu^{243}.[58,59] The cross section for the formation of Pu^{243} by the reaction $Pu^{242}(n,\gamma)Pu^{243}$ with slow neutrons has been determined[59] as approximately 100 barns.

A mixture of Pu^{242} and Pu^{238} was irradiated for a short time in the Hanford nuclear reactor, and the plutonium fraction was subsequently repurified by K. Street, Jr. and D. A. Orth. This sample, now containing Pu^{243}, was mounted on a thin Tygon film and investigated in the beta spectrometer. Unfortunately, the specific activity of the source was very low; the spectrometer detector indicated only about 110 counts/minute above background at the peak of the beta distribution. Although fairly long counts were made, the statistics were limited to 10-15 percent because of the 5 hour half-life. A Fermi-Kurie plot of the smoothed data is shown in Figure 24, in which the beta energy is found to be 0.41 ± 0.02 Mev.

Ghiorso finds two gamma rays of approximately 0.1 Mev energy,[60] from pulse analysis of the electromagnetic radiation using a xenon filled proportional counter. Because of the low activity of the Pu^{243} source, a thorough search for conversion electrons could not be made manually on the beta spectrometer, so the motor driven sweep was employed. Two rather questionable peaks were seen in the region of L electrons from gamma rays of about 0.1 Mev; if these lines are L electron lines the gamma ray energies are 0.095 and 0.12 Mev.

Making the assumption that the two gamma rays are in cascade, one obtains a disintegration energy of about 0.6 Mev for Pu^{243}, from which the alpha particle energy of Pu^{243} can be calculated by closing the

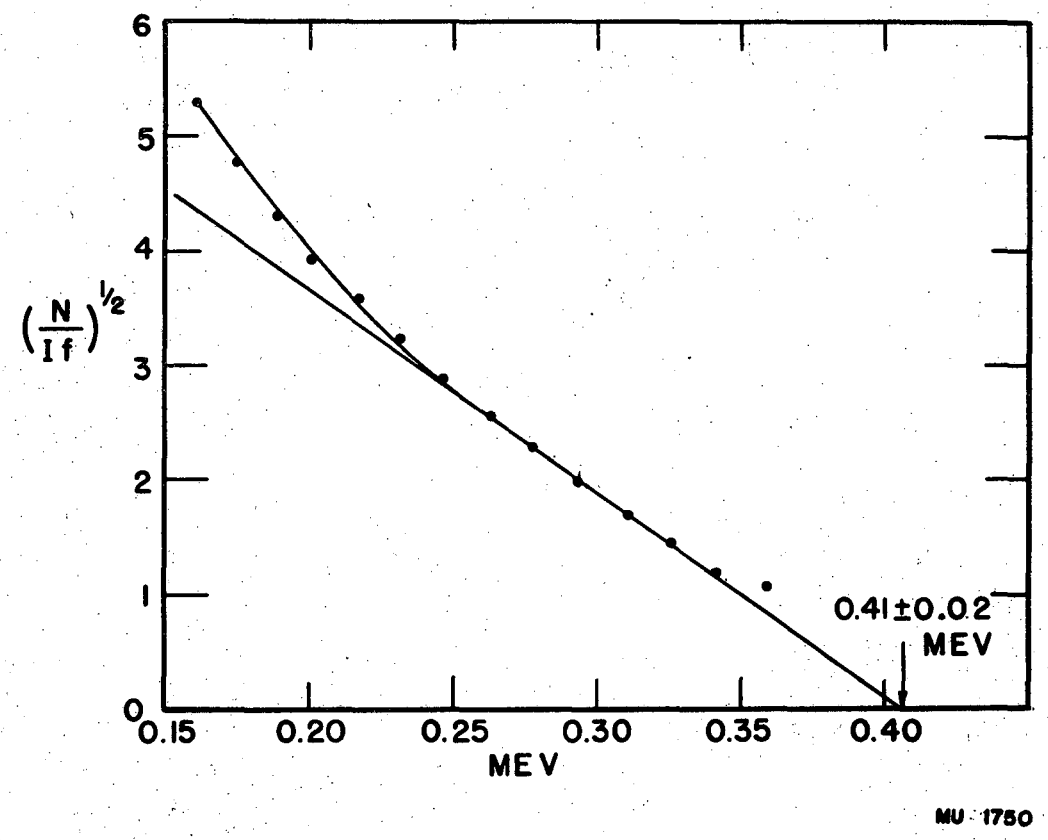

Fig. 24

Fermi-Kurie plot of Pu^{243} beta spectrum

decay cycle:

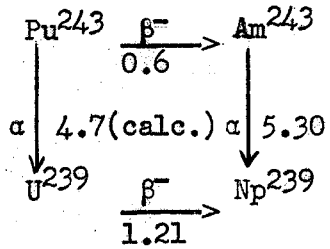

However, it is possible that the beta spectrum is complex and that the beta decay energy of Pu^{243} is actually 0.5 Mev; this would lead to an alpha particle energy of 4.6 Mev for Pu^{243}, which is not as consistent with the alpha systematics as the 4.7 Mev value.

After the decay of the 5 hour Pu^{243} activity, some low energy electron lines remained which had not decayed appreciably. These lines are attributed to Pu^{238}, since the nuclides Pu^{242} and Pu^{239} also present in the source are too long lived to have been detected in this experiment.

The electron spectrum without counter window correction is shown in Figure 25. A table of electron energies and their possible interpretation is tabulated below:

E, Kev	Interpretation	E_γ, Kev
23	L_{Ia} + Auger	44.8
24.2	L_{IIa}	45.2
25.9 (?)	L_{Ib} (?)	47.7
27.9	L_{IIIa}	45.1
31.1 (?)	L_{IIIb} (?)	48.3
40.9	M_{IIIa}	45.2
45.9	M_{Vb} (N_a + O_a ?)	48.6

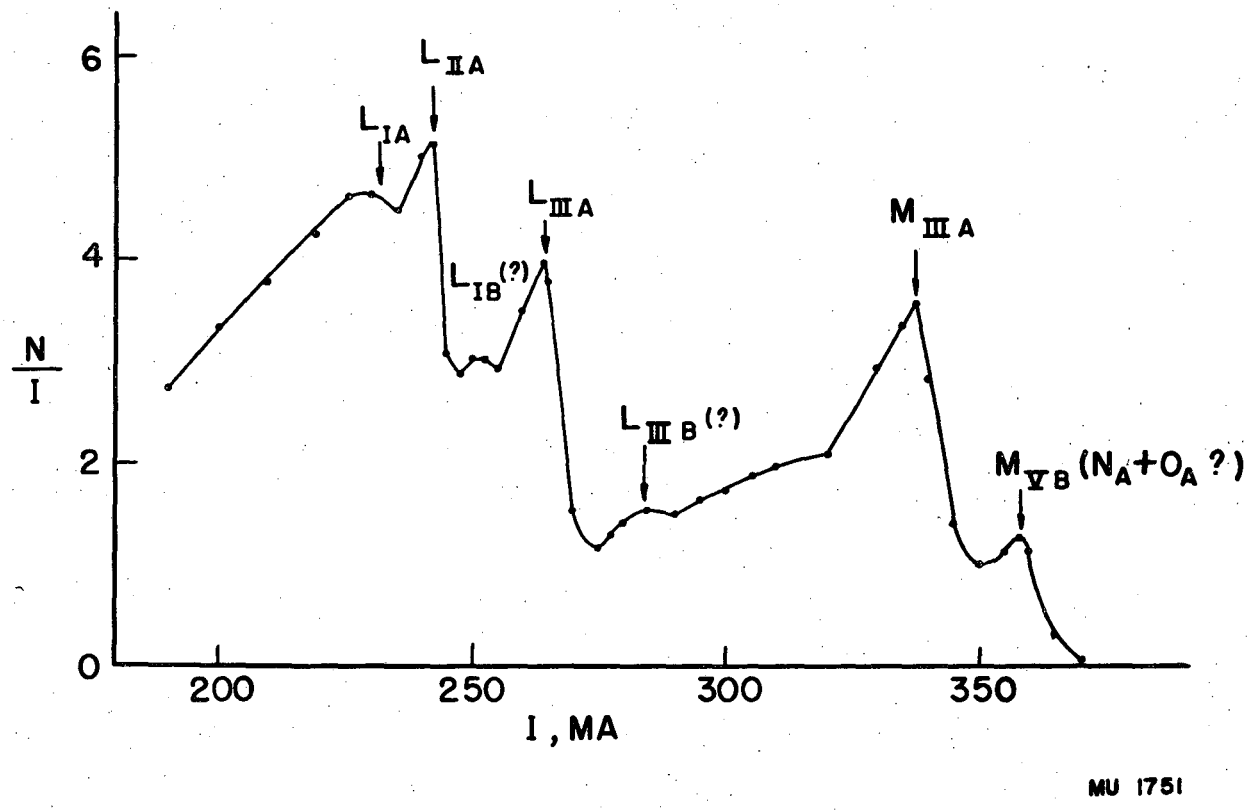

Fig. 25

Electron spectrum of Pu^{238}

The L and M internal conversion lines are definitely assigned, but the lines indicated as questionable are difficult to intrepret. However, one may be fairly certain of the existence of two gamma rays in Pu^{238}, with energies of 45.1 ± 0.5 Kev, and about 48 Kev. No attempt was made to measure relative abundances of the various lines. It must be recalled that in the figure no window absorption corrections were applied, so the low energy lines are actually in much higher abundance.

F. Radiations of Pb^{203} and Pb^{200}

A study of 52 hour Pb^{203} provides an opportunity to look for a transition in the Tl^{203} daughter common to the transition observed when Tl^{203} is excited by the beta decay of Hg^{203}. Slätis and Siegbahn[61] have carefully investigated Hg^{203}, and find K and L internal conversion lines of a single 279 Kev gamma ray with a ratio of K to L electrons of about 3. Lutz, Pool, and Kurbatov[62] found electron lines of a 270 gamma ray in the decay of Pb^{203}, as well as a line which they assigned to Compton electrons from a 470 Kev gamma ray. It thus seemed worthwhile to investigate the decay of Pb^{203} more thoroughly in the hope that either this discrepancy could be resolved or established.

The first sample investigated was prepared by the (d,2n) and (d,4n) reactions on thallium, using 60 Mev deuterons from the 184 inch cyclotron. The chemically separated lead fraction was prepared by D. G. Karraker, and contained only about 50 μgms of lead as carrier.

The Geiger counter tube used in the experiments had a mica window about 3 mg/cm^2 thick, so rather severe window absorption was encountered at some of the very low energies. A preliminary sweep indicated

that the peaks were all below 0.35 Mev. The elctron spectrum below this energy is shown in Figure 26, which demonstrates the complexity of the mixture. Realizing that there was a considerable quantity of 18 hour Pb^{200} present from the reaction $Tl^{203}(d,5n)Pb^{200}$, the decay of the prominent electron lines was followed. A run about three days later is shown in Figure 27, in which several lines have definitely decayed with a shorter half-life. On this basis, K_1, L_1, and M_1 are assigned to a 0.139 Mev gamma ray of Pb^{200}, while K_2, L_2, and M_2 are the internal conversion electrons of the 0.269 Mev gamma ray of Pb^{203}. The lines K_3 and L_3 decay at about the same rate as L_1, and correspond to internal conversion lines of a 0.320 Mev gamma ray of Pb^{200}. The line K_4 is longer lived than L_3 and seems to decay with about the same half-life as the L line of the 0.269 Mev gamma ray of Pb^{203}. Since all other lines in this energy region can be accounted for, K_4 is probably the K line of a 0.424 Mev gamma ray. Further, as the lines due to the soft 0.139 Mev gamma ray of Pb^{200} decrease in intensity, a new line, K_5 is noted. It is assumed that this is the K line of a third gamma ray of Pb^{203}, having an energy of 0.153 Mev.

Thus one is led to postulate a decay scheme in which the electron capture in Pb^{203} excites a level about 0.422 Mev above the ground state of Tl^{203}, and that this state emits either a 0.422 Mev gamma ray, or a 0.269 Mev and a 0.153 Mev gamma ray in cascade.

The measurement of Lutz, Pool, and Kurbatov[62] is therefore confirmed for the 0.269 Mev gamma ray, and it appears that the beta decay of Hg^{203} and the electron capture in Pb^{203} indeed excite different energy levels. Also, the decay scheme of Pb^{203} is considerably more complicated

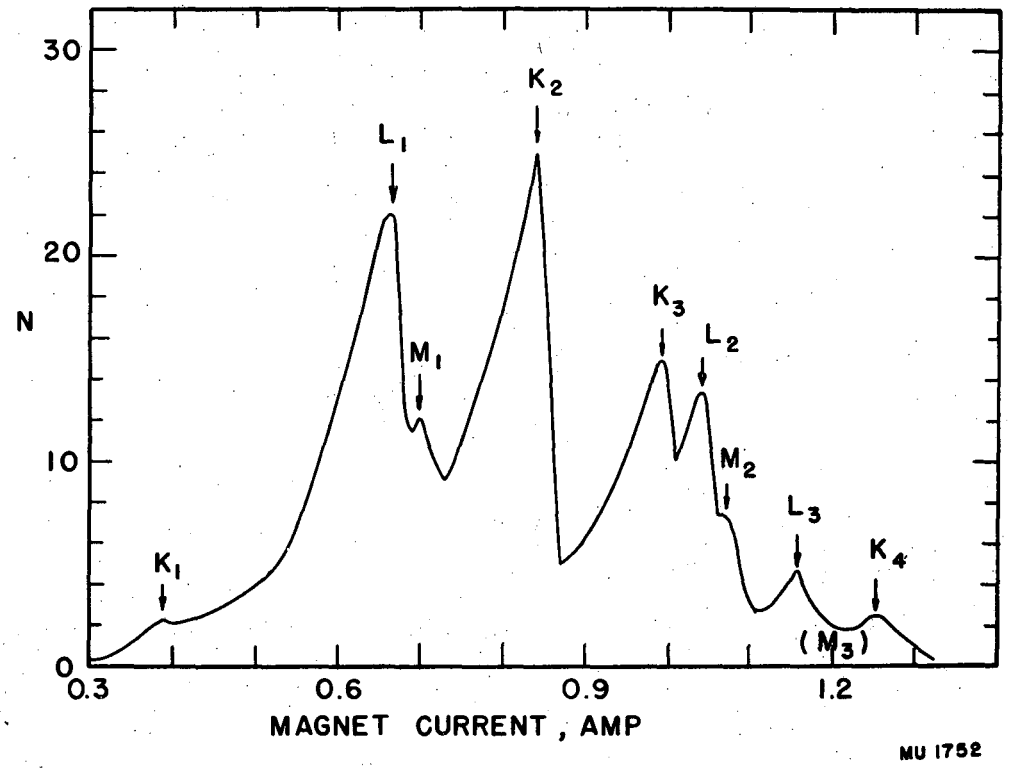

Fig. 26

Electron spectrum of $Pb^{200,203}$ mixture

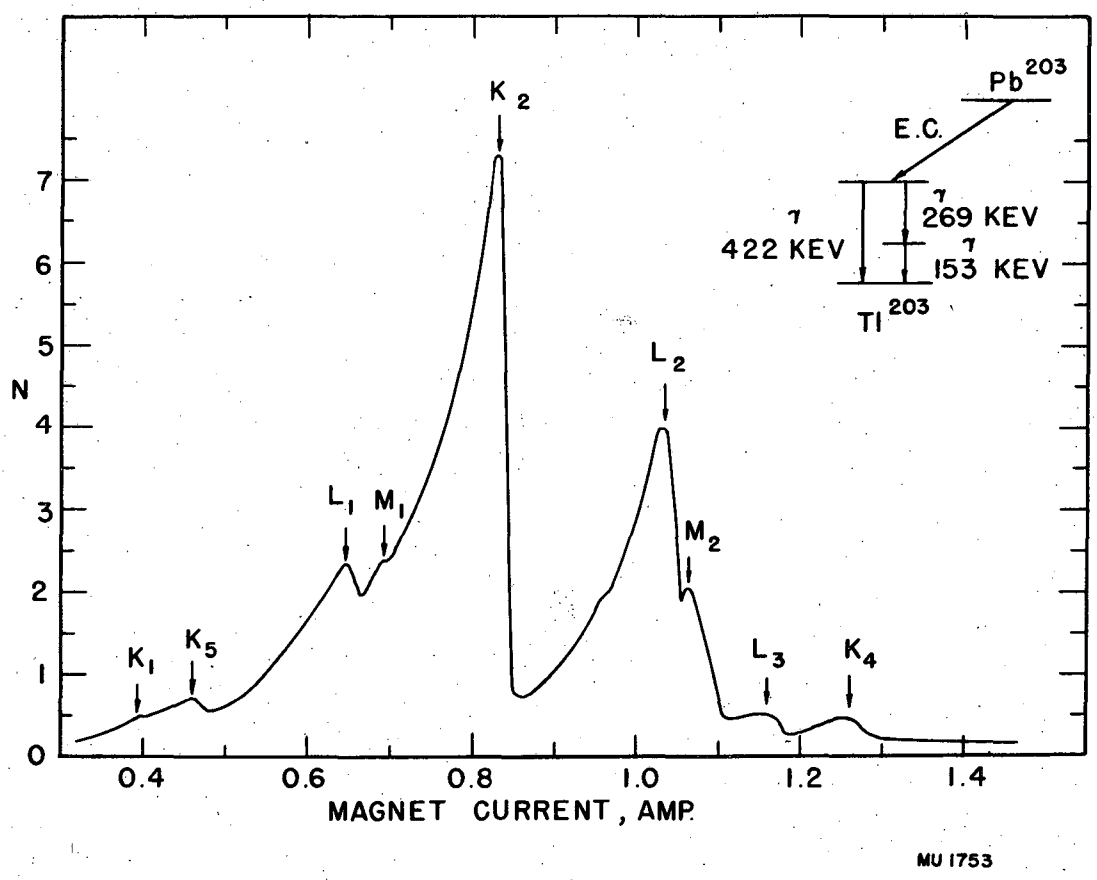

Fig. 27

$Pb^{200,203}$ electron spectrum, observed three days after Fig. 26. Also shown is the decay scheme proposed for Pb^{203}.

than the Hg^{203} decay. Further evidence that the 0.269 Mev gamma ray and the 0.279 Mev gamma ray represent different transitions is seen from the ratio of K electrons to L electrons. Slätis and Siegbahn[61] report $N_K/N_L = 3$ for the Hg^{203} gamma ray, while the 0.269 Mev gamma ray of Pb^{203} has a $N_K/N_L = 2.3$ after correcting for absorption in the counter window. It is possible that this variation represents a significant difference in the character of the radiations.

No internal conversion electrons were seen which could be interpreted as lines of a 0.47 Mev gamma ray from the decay of Pb^{203}. However, Lutz, Pool, and Kurbatov[62] obtained this gamma ray energy from the endpoint of a Compton electron distribution, uncorrected for spectrometer resolution. This procedure is known to give high results[63] and it is possible that this gamma ray is actually the 0.424 Mev gamma ray observed in these experiments. The decay scheme proposed for Pb^{203} is included in Figure 27.

G. Beta Energy of Pb^{209}

The disintegration energy of Pb^{209} is especially interesting because of the apparent descrepancy arising from a cycle involving the neutron binding energies of Pb^{207}, Pb^{208}, Pb^{209}, Bi^{210}, and the decay energies of Pb^{209}, Bi^{210}, and Po^{210}. Consider the following closed cycle:

$$Pb^{206} + M_n = Pb^{207} + 6.70 \text{ Mev}$$
$$Pb^{207} + M_n = Pb^{208} + 7.37$$
$$Pb^{208} + M_n = Pb^{209} + 3.88$$
$$Pb^{209} = Bi^{209} + E_{\beta 1}$$
$$Bi^{209} + M_n = Bi^{210} + 4.18$$
$$Bi^{210} = Po^{210} + E_{\beta 2}$$
$$Po^{210} = Pb^{206} + M_\alpha + 5.30 \text{ Mev}$$

Adding the above equations, the heavy masses cancel, and there remains

$$4M_n - M_\alpha = 27.43 + E_{\beta 1} + E_{\beta 2}$$

Using values for $E_{\beta 1}$ and $E_{\beta 2}$ of 0.66 and 1.17 Mev respectively, the right member becomes 29.36 Mev, compared with 29.81 Mev for the left member. The neutron binding energies used were those of Harvey,[64] while the Bi^{210} (RaE) and Po^{210} energies have been widely investigated and may be considered well known. Thus a discrepancy of about 0.4 Mev results if the disintegration energy of Pb^{209} is taken as 0.66 Mev.

Harvey[64] believes this discrepancy is due to a gamma ray of about 0.4 Mev which follows the beta transition. The purpose of the experiment to be described was to look for internal conversion electrons corresponding to gamma rays of about this energy, and to remeasure the beta energy.

The sample of Pb^{209} activity was prepared by irradiation of ordinary lead with 18 Mev deuterons from the Crocker Radiation Laboratory cyclotron and was chemically purified by H. M. Neumann. Since the sample was not carrier free, the beta spectrometer source was quite thick (several mg/cm^2), and low energy lines could not have been seen. No electron lines were detectable up to 1.0 Mev. Neumann found no evidence for a gamma ray of about 0.4 Mev, using absorption techniques;[65] the aluminum absorption curve of the beta particles dropped a factor of 1200 to bremsstrahlung, indicating that any gamma rays present were of low abundance. However, any gamma ray postulated to be present in low abundance would not be in cascade with the main beta group, and hence would not resolve the question of the supposedly low decay energy of Pb^{209}.

A Fermi-Kurie plot of the beta spectrum is shown in Figure 28, and is apparently complex, with beta components of 0.66 ± 0.01 Mev and 0.53 ± 0.01 Mev. It is obvious from the Fermi-Kurie plot that the source was thick, at least in spots, because of the sudden absorption effect at about 300 Kev, causing the curve to drop toward the energy axis. Because of the thick source, the K line from a possible 0.13 Mev gamma ray could not have been seen, and the L line might have been in such low abundance that it was missed. It is therefore reasonable to find a two component beta spectrum without seeing the associated gamma ray. However, it must be stated that no effort was made to correct for the thick source after the manner of Owen and Primakoff,[17] since one would expect the Fermi-Kuri plot to be affected at energies considerably below 0.5 Mev.

Thus, it is difficult to account for the discrepancy in the closed cycle by a higher Pb^{209} decay energy. The most probable source of error would seem to be the measurements of the neutron binding energies. Harvey's value of 3.88 Mev for the binding of a neutron between Pb^{208}-Pb^{209} constitutes the only measurement of this quantity. The other energies used in the closed cycle calculation have been found by at least two investigators and are believed to be more accurate. However, Kinsey[66] reports that the gamma ray peak from the (n,γ) reaction on Bi^{209} is very broad, which may indicate that his measurement as well as Harvey's measurement might not involve the ground state transition and would hence be low.

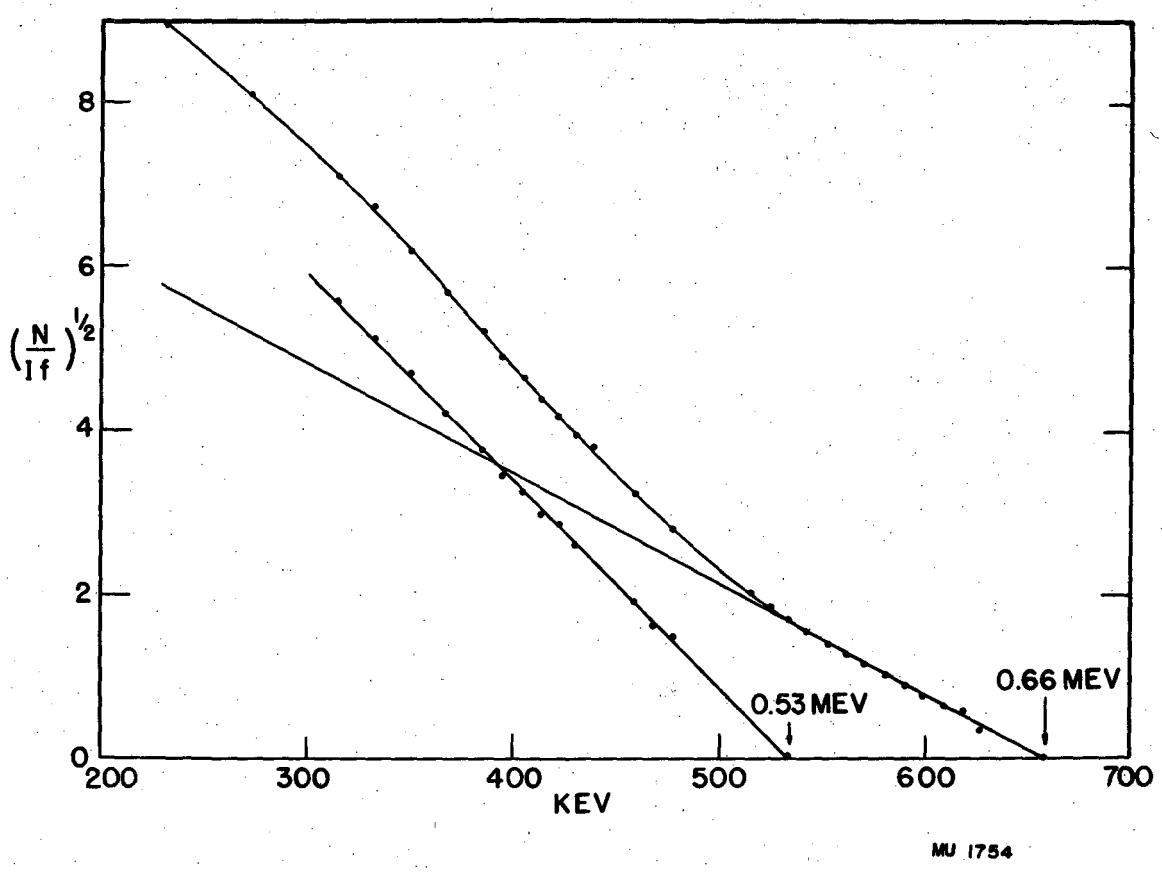

Fig. 28

Fermi-Kurie plot of Pb^{209} beta spectrum

H. Neutron Deficient Isotopes of Zirconium and their Decay Products

This section concerns work done with Dr. E. K. Hyde, who has established radiochemically the decay schemes discussed below. The present author's work on the energies of the various decay processes will be treated here. A more detailed account of the radiochemical and spectroscopic research will be published.[67]

It is possible to prepare a number of the lighter neutron deficient isotopes of zirconium by bombarding high purity niobium metal with 100 Mev protons in the 184-inch cyclotron. The lightest molybdenum and niobium isotopes produced by (p,xn) and (p,pxn) reactions decay quickly by electron capture or positron emission to isotopes of zirconium. Also, zirconium isotopes may be produced by spallation reactions of the type $Nb^{93}(p,2pxn)Zr^{<93}$. Such reactions allow preparation of isotopes of zirconium of mass number 89 or less, free from higher mass zirconium activities.

Zirconium 87.--The decay scheme which best fits the information for Zr^{87} is presented in Figure 29. The decay curve of a zirconium fraction from a proton irradiated niobium target is complex. A prominent activity with a half-life of about 90 minutes is observed, although reliable resolution of the curve is difficult because the growth and decay of yttrium and strontium daughter activities is superimposed upon the straight decay of 78 hour Zr^{89}, 17 hour Zr^{86}, and the short lived activity which is due to Zr^{87}. The nature and energies of the radiations did not allow simplification of the resolution by following the decay through properly selected absorbers. The half-life

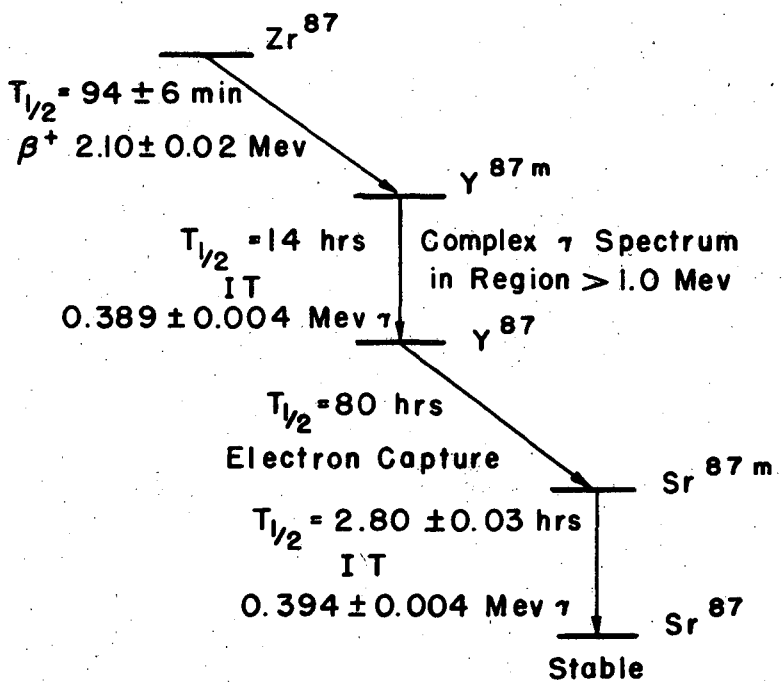

Fig. 29

Decay scheme of Zr^{87}

of Zr^{87} was measured by placing a sample in the beta spectrometer and following the decay of positrons of an energy greater than the 0.910 Mev positrons of Zr^{89}. A typical decay curve is shown in Figure 30. The points have been corrected for counter background. As a result of several determinations a value of 94 ± 6 minutes is obtained for the half-life of Zr^{87}. This value is considerably shorter than the 120 ± 6 minute half-life found by Robertson et al.[68]

In preparation for a measurement of the Zr^{87} positron energy, the beta spectrometer was calibrated with the K internal conversion line of the Cs^{137} gamma ray, and the calibration was checked by determining the energy of the P^{32} beta particle. A value of 1.685 ± 0.01 Mev was obtained, in excellent agreement with the recent value of Langer and Price.[69] The resolution of the spectrometer was 1.5 percent.

The Fermi-Kurie plot of the Zr^{87}-Zr^{89} mixture was resolved into the 2.10 ± 0.02 Mev component of Zr^{87} and the 0.910 ± 0.010 Mev component of Zr^{89} and no others. The portion of the plot beyond the endpoint of Zr^{89} is shown in Figure 31. The value for Zr^{87} agrees with that of Robertson et al.[68] within the experimental error of their absorption measurements.

An examination of the electron spectrum showed no prominent conversion electrons which could be assigned to Zr^{87}. In addition, Hyde found no evidence for Zr^{87} gamma radiation, using lead absorption techniques on freshly purified zirconium fractions; however, it was not possible to set very low limits by either method. Robertson et al.[68] found gamma rays of 0.35 and 0.65 Mev energy, and x-radiation

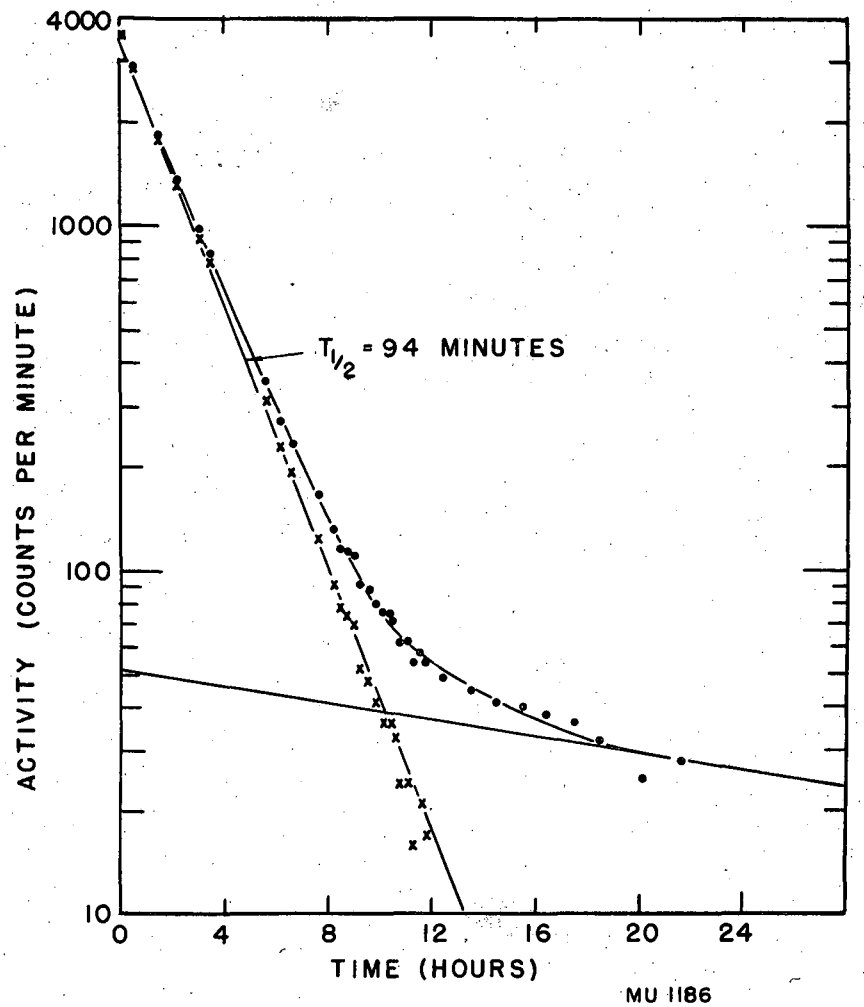

Fig. 30

Half-life of Zr^{87} determined by measuring decay of monoenergetic positrons of 1.47 Mev in the beta spectrometer

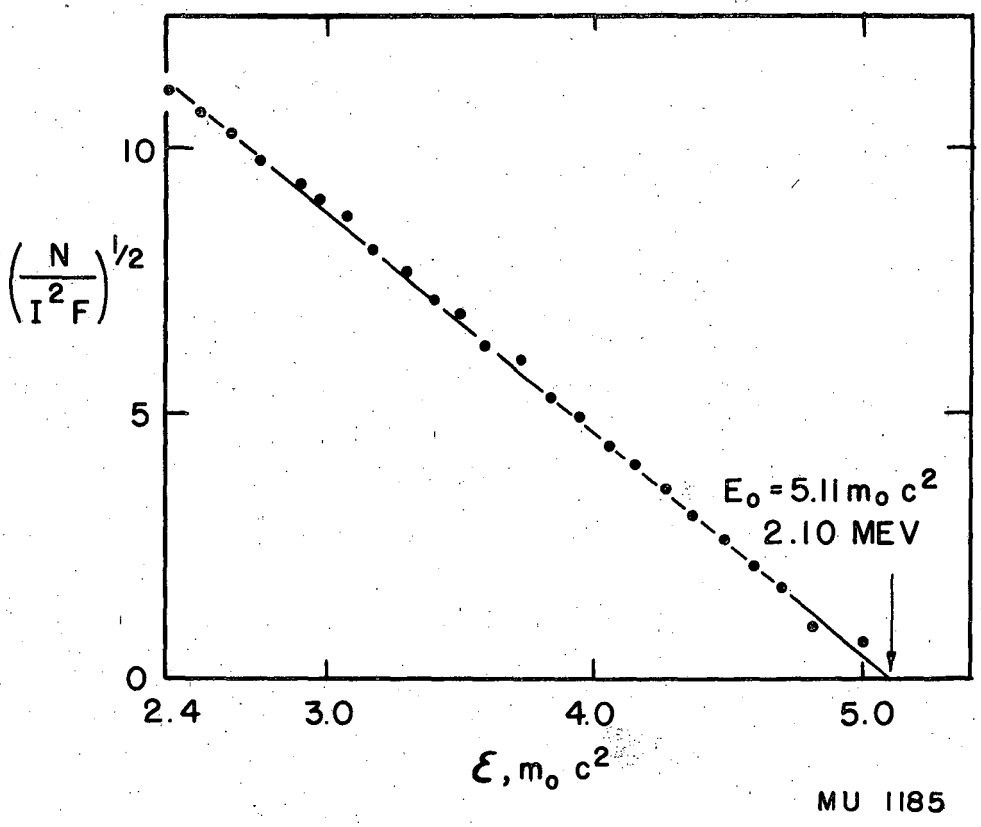

Fig. 31

Fermi-Kurie plot of high energy portion of Zr^{87} positron spectrum

accompanying Zr^{87} decay.

Decay Products of Zr^{87}.--If an yttrium fraction is separated from the purified zirconium within two or three hours after bombardment, the yttrium fraction is almost 100 percent Y^{87m} with a nearly undetectable trace of Y^{86} and Y^{88}. Radiochemical evidence indicates[67] that the Y^{87m} undergoes isomeric transitions, forming Y^{87}. The ground state Y^{87} decays by pure electron capture to Sr^{87m}, which in turn emits a single gamma ray to form stable Sr^{87}.

Carrier free samples of Y^{87m} freshly isolated from the Zr^{87} parent were mounted on thin Tygon films and examined in the beta spectrometer. The most prominent radiations were the conversion lines (Figure 32) of the 0.389 Mev gamma ray. The K/L ratio was 8.3 ± 0.5. The half-life and K/L ratio suggest electric 2^5 pole radiation.

Mann and Axel[70] have measured the K conversion line of this gamma ray to be 0.374 Mev, which would indicate a gamma ray energy of 0.391 Mev. However, they state that in only 50 percent of its disintegrations does Y^{87m} decay by isomeric transition, while in half the disintegrations Y^{87m} decays directly to Sr^{87m}. They place the 0.39 Mev gamma ray in this transition. It is difficult to fit the radiochemical evidence of Hyde and O'Kelley[67] to this scheme.

Robertson et al.[68] report that 14 hour Y^{87m} decays by positron emission and not by isomeric transition and state that Y^{87m} and Y^{87} decay independently to Sr^{87m}. From the evidence below, this cannot

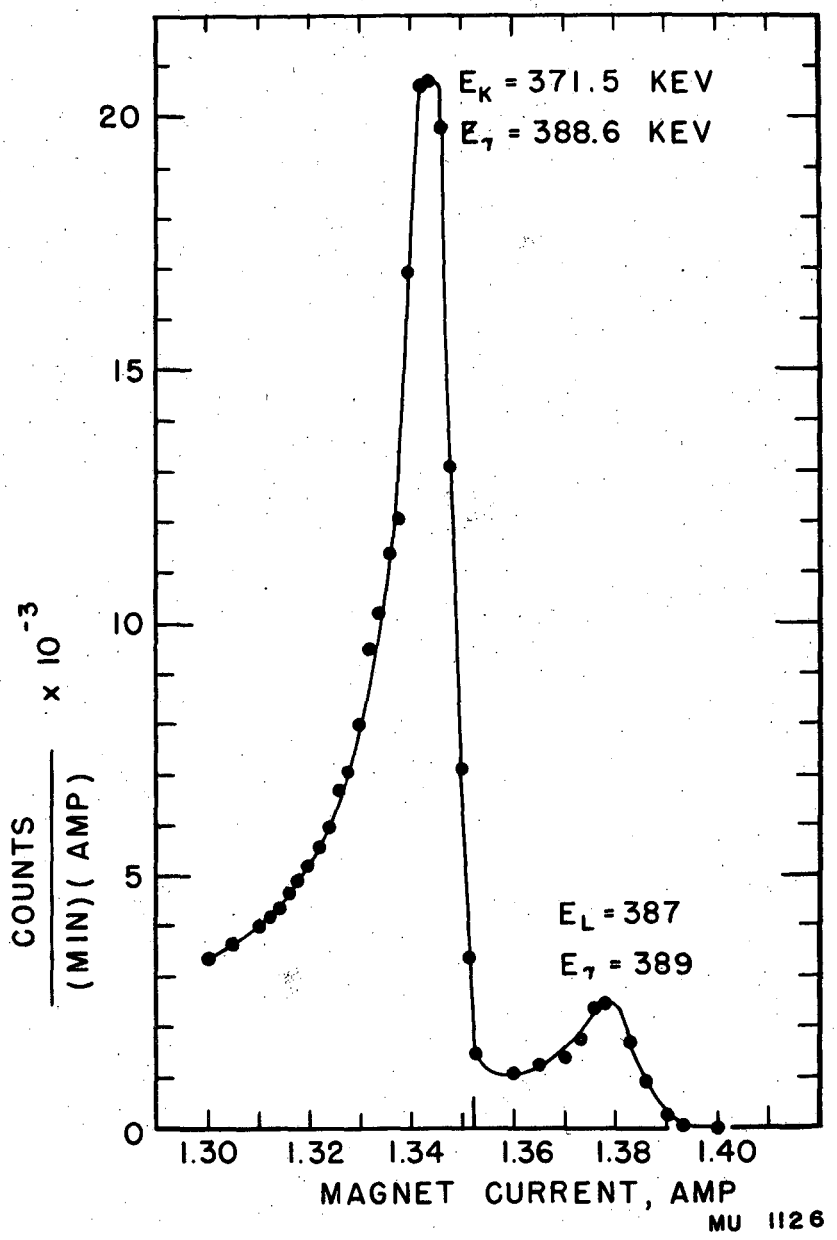

Fig. 32

Conversion electrons of the 0.389 Mev gamma ray of Y^{87m}

be the case. It is possible that Robertson and co-workers were measuring the 14.6 hour yttrium activity which is assigned to Y^{86} (see below), which in their bombardments would have appeared through the $Sr^{84}(\alpha,pn)Y^{86}$ reaction.

Figure 33 shows the decay of the conversion electrons of the Y^{87m} gamma ray, and the growth of the conversion electrons of the Sr^{87m} granddaughter. Figures 32 and 33 represent the same sample examined approximately 3 hours, 28 hours, and 45 hours after preparation of the pure Y^{87m} sample. The Sr^{87m} gamma ray energy is 0.394 ± 0.004 Mev, and is definitely higher in energy than the gamma ray of Y^{87m} (Figure 32). Mann and Axel[70] report the Sr^{87m} gamma ray energy to be 0.390 Mev. The K/L ratio of the Sr^{87m} gamma ray is 7.2 which is in agreement with Mann and Axel's[70] value of 6.9, within experimental error.

Within experimental error, the area under the K line of Y^{87m} decayed with the proper 14 hour half-life. The sum of the areas under all four peaks of Figure 33 decayed in a manner similar to the curve expected for a 14 hour decay plus the growth and decay of a 2.80 hour granddaughter having a counting efficiency (conversion coefficient) about 20 percent lower than the 14 hour activity. In this calculation it was assumed that the daughter of the 14 hour activity was counted with zero counting efficiency. This indicates that the Sr^{87m} is formed completely through the 0.389 Mev transition in Y^{87m}, and that the decay scheme of Figure 29 is correct. Similar results are obtained when an ordinary Geiger counter is used to follow the decay, since the conversion electrons of Y^{87m} and Sr^{87m} are counted

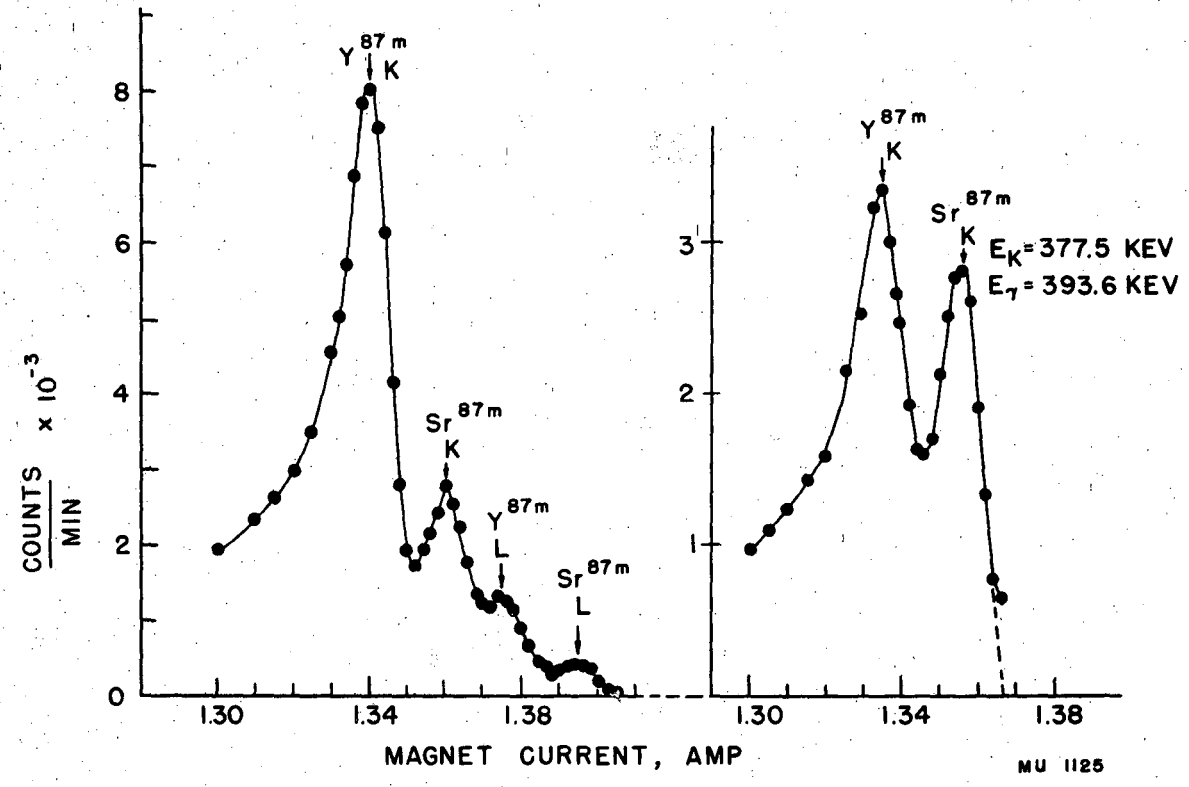

Fig. 33

The conversion electron spectrum 28 hours and 46 hours after preparation of the pure Y^{87m} sample, showing growth of conversion electrons of 0.394 Mev gamma ray of Sr^{87m}

efficiently, while the x-rays from the electron capture in Y^{87} are not detected appreciably.

In addition to these prominent lines, an examination of the electron spectrum of freshly prepared Y^{87m} showed eight internal conversion lines in the region above 1 Mev. Tentatively, these are assigned to gamma rays of 1.07, 1.15, 1.44, 1.49, 1.54, 1.60, 1.66, and 1.71 Mev energy. No detailed study has been made of these electrons but they appear to decay with a 14 hour half-life. The total number of positrons was <0.001 times the number of conversion electrons. No conversion electrons were observed for the 80 hour Y^{87} other than Auger electrons. Lead absorption measurements on Y^{87m} show considerable hard gamma radiation of energy greater than 1 Mev, but no hard radiation is found for Y^{87} or Sr^{87m}. Mann and Axel report that the K capture decay is followed by the emission of a 0.485 Mev gamma ray. We failed to see these conversion electrons in our spectrometer studies, but the conversion coefficient reported by these authors is so small that they could have been overlooked in these experiments.

Zirconium 89.--If a purified zirconium fraction from proton bombarded niobium is allowed to decay for several days, it is found that 78 hour Zr^{89} is the predominant activity remaining after repurification. By this time the other zirconium activities have decayed out with the exception of Zr^{88}, which because of its long half-life and inefficiently counted x-radiation contributes only a few percent to the total radiation at this time.

Carrier free Zr^{89} samples were examined in the spectrometer. A Fermi-Kurie plot of the positron spectrum gave a value of 0.910 ± 0.010 Mev. This value is lower than the value of 1.07 Mev obtained by Overstreet, Jacobson, and Hamilton by aluminum absorption.

Four groups of conversion electrons were observed, corresponding to gamma ray energies of 0.027 ± 0.001, 0.396 ± 0.004, 0.917 ± 0.005, and 1.27 ± 0.01 Mev. The electron spectra of the last three gamma rays are shown in Figure 34. It is apparent that the decay scheme of Zr^{89} is complex, although it seems probable that a single positron transition occurs to a level about 1.31 Mev above the ground state of Y^{89}, and that this excited state decays either by the emission of 0.396 and 0.917 Mev gamma rays in cascade, or by 1.27 and 0.027 Mev gamma rays in cascade.

Yttrium 86.--If a purified zirconium fraction is allowed to decay for about a day and then repurified, no more of the mass 87 chain daughters are formed. Subsequent removal of an yttrium fraction after the remaining zirconium had decayed for another day yields considerable Y^{86} positron activity, which decays with a half-life of 14.6 ± 0.2 hours.[67] Less than 0.1 percent of the yttrium activity is due to Y^{88}. The nuclide Y^{86} was discovered by Castner[72] in bombardments of strontium isotopes. Lead absorption experiments indicate a hard gamma ray of 1.4 Mev.[67]

A Fermi-Kurie plot of the positron spectrum of Y^{86} is shown in Figure 35. The data are corrected for instrumental distrotion according to Owen and Primakoff.[17] Two components are present in about equal

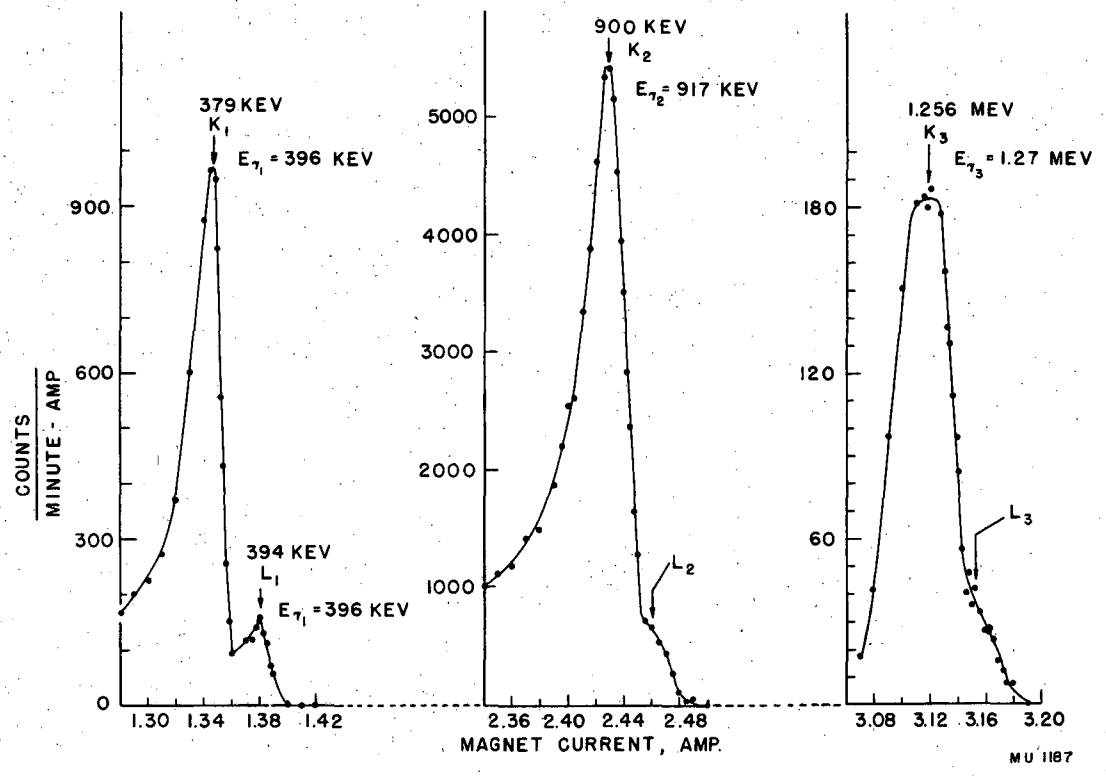

Fig. 34

Conversion electrons of Zr^{89}

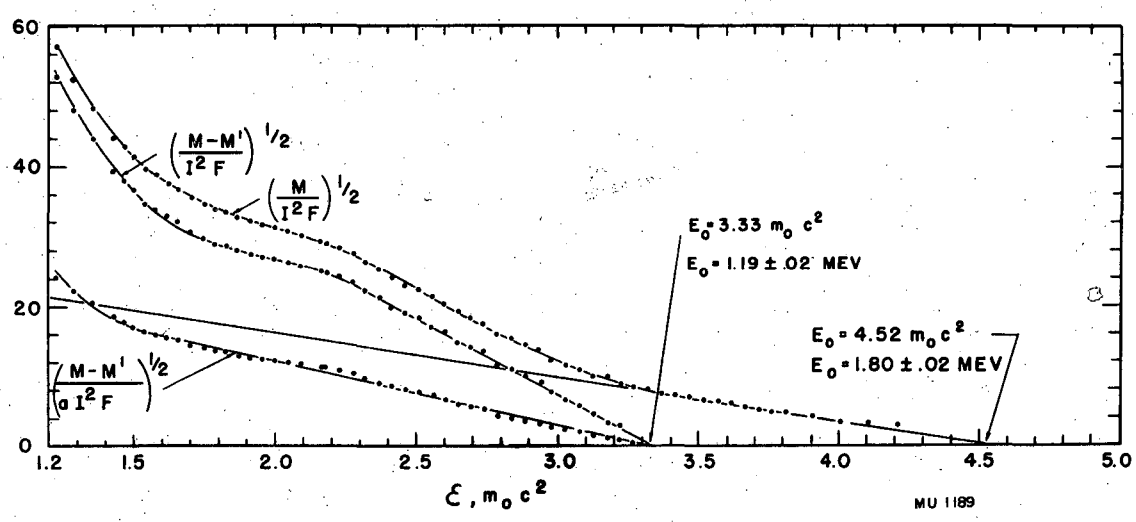

Fig. 35

Fermi-Kurie plot of Y^{86} positron spectrum

intensity, with maximum energies of 1.80 ± 0.02 and 1.19 ± 0.02 Mev. There are not sufficient data on the high energy component to establish its shape, but the low energy group appears to be forbidden. The comparative half-life of the low energy positron ($ft \sim 10^6$) indicates a first forbidden transition, while the spectral shape suggests a spin change of two units and a change of parity. According to the theory of forbidden spectra,[73,74] dividing the ordinates of the plot of the low energy component of Figure 35 by $a^{1/2}$ should yield a straight line if the transition is of this type. The factor $a = (\varepsilon^2 - 1) + (\varepsilon_o - \varepsilon)^2$, with ε the energy in units of $m_o c^2$, arises from the unique energy dependence of the transition. Figure 35 shows such a corrected plot, and it is seen that a straight line does result.

The factor $c = (\varepsilon^2 - 1)^2 + 10/3(\varepsilon^2 - 1)(\varepsilon_o - \varepsilon)^2 + (\varepsilon_o - \varepsilon)^4$ gave a poor fit. Conformity to this factor would have indicated a second forbidden transition with a spin change of three units and no change in parity.

Internal conversion conversion lines were sought, but none were seen. However, the samples were of comparatively low intensity, and the presence of gamma radiation other than a hard 1.4 Mev gamma ray seen in lead absorption experiments cannot be ruled out.

IV. ACKNOWLEGMENT

The work described in this dissertation was performed under the direction of Professor G. T. Seaborg, whose thoughtful advice and encouragement are gratefully acknowleged.

The assistance and advice of Mr. F. L. Reynolds in the construction and operation of the beta spectrometer is greatly appreciated. I wish to thank Mr. A. Garren for the design of the beta spectrometer magnet polepieces, Mr. H. P. Hernandez for the engineering design of the magnet assembly, Messrs. H. D. Farnsworth and E. Powers for supplying the necessary electronic equipment.

I am indebted to Professor I. Perlman for many suggestions and discussions, and to Dr. E. K. Hyde, Mr. W. W. T. Crane, Dr. D. A. Orth, Dr. D. G. Karraker, Dr. H. M. Neumann, Dr. G. W. Barton, and Mr. C. I. Browne, Jr., for assistance in many of the experiments.

This work was performed under the auspices of the U. S. Atomic Energy Commission.

V. REFERENCES

1. G. T. Seaborg and I. Perlman, Revs. Modern Phys. 20, 585-677 (1948).
2. C. Allan and G. Mitchell, Revs. Modern Phys. 22, 36 (1950).
3. I. Perlman, A. Ghiorso, and G. T. Seaborg, Phys. Rev. 77, 26 (1950).
4. I. Perlman, Nucleonics 7, No. 2, 3 (1950).
5. S. G. Thompson, Phys. Rev. 76, 319 (1949).
6. L. M. Langer and C. S. Cook, Rev. Sci. Inst. 19, 257 (1948).
7. E. Fermi, Zeit. f. Physik 88, 161 (1934).
8. G. Gamow and E. Teller, Phys. Rev. 49, 895 (1936).
9. E. P. Wigner, Phys. Rev. 56, 519 (1939); see also L. W. Nordheim and F. L. Yost, Phys. Rev. 51, 942 (1937).
10. E. Feenberg and K. C. Hammack, Phys. Rev. 75, 1877 (1949).
11. E. J. Konopinski, Revs. Modern Phys. 15, 209 (1943).
12. L. W. Nordheim, Los Alamos Scientific Laboratory Report NP-1769 (May, 1950).
13. E. Feenberg and G. Trigg, Revs. Modern Phys. 22, 399 (1950).
14. F. N. D. Kurie, J. Richardson, and H. Paxton, Phys. Rev. 49, 368 (1936).
15. H. A. Bethe and R. F. Bacher, Revs. Modern Phys. 8, 194 (1936).
16. I. Feister, Phys. Rev. 78, 375 (1950).
17. G. E. Owen and H. Primakoff, Phys. Rev. 74, 1406 (1949); Rev. Sci. Inst. 21, 447 (1950).
18. C. S. Wu and L. Feldman, Phys. Rev. 76, 698 (1949).
19. E. Segrè and A. C. Helmholz, Revs. Mod. Phys. 21, 271 (1949).
20. H. A. Bethe, Revs. Modern Phys. 9, 220 (1937).
21. P. Axel and S. M. Dancoff, Phys. Rev. 76, 892 (1949).

22. H. R. Hulme, Proc. Roy. Soc. (London) A138, 643 (1932).

23. G. Goertzel and M. E. Rose, U. S. Atomic Energy Commission Report MDDC-1514 (November, 1947).

24. M. E. Rose, G. H. Goertzel, B. I. Spinrad, J. Harr, and P. Strong, Phys. Rev. 76, 184 (1949).

25. H. Gellman, B. A. Griffith, and J. P. Stanley, Phys. Rev. 80, 866 (1950).

26. J. Danysz, Compt. rend. 153, 339 (1911).

27. P. Kapitza, Proc. Comb. Phil. Soc. 22, Pt. 3 (1925).

28. R. A. R. Tricker, Proc. Comb. Phil. 22, 454 (1925).

29. N. Svartholm and K. Siegbahn, Arkiv Mat. Astron. Fys., 33A, No. 21 (1946); Nature 157, 872 (1946).

30. N. Svartholm, Arkiv Mat. Astron. Fys. 33A, No. 24 (1946).

31. A. Hedgran, K. Siegbahn, and N. Svartholm, Proc. Phys. Soc. 63A, 960 (1950).

32. F. B. Shull and D. M. Dennison, Phys. Rev. 71, 681 (1947); 72, 180 (1947); 72, 256 (1947).

33. F. B. Shull, Phys.Rev. 74, 917 (1948).

34. F. N. D. Kurie, J.S.Osoba, and L. Slack, Rev. Sci. Inst. 19, 771 (1948).

35. E. Persico and C. Geoffrion, Rev. Sci. Inst. 21, 945 (1950).

36. J. D. Cockcroft, J. Sci. Inst. 1, No. 3 (1933).

37. A. Guthrie and R. K. Wakerling, Vacuum Equipment and Technique, National Nuclear Energy Series, Division I, Electromagnetic Separation Project Record, Vol. I. New York: McGraw-Hill, Inc. (1950).

38. G. T. Seaborg, R. James, and L. O. Morgan, The Transuranium Elements: Research Papers, National Nuclear Energy Series, Plutonium Project Record 14B, Paper No. 22.1, New York: McGraw - Hill Book Company, Inc. (1949).

39. W. M. Manning and L. B. Asprey, ibid, Paper No. 22.7.

40. S. G. Thompson, K. Street, Jr., A. Ghiroso, and F. L. Reynolds, University of California Radiation Laboratory Report UCRL-657 (June, 1950); Phys. Rev. 80, 1108 (1950).

41. G. W. Barton, Jr., H. P. Robinson, and I. Perlman, Phys. Rev. 81, 208 (1951).

42. A. H. Compton and S. K. Allison, X-Rays in Theory and Experiment, Second Edition, p. 800. New York: D. Van Nostrand Company, Inc. (1935).

43. W. W. T. Crane and A. Ghiorso, unpublished data.

44. D. A. Lind, W. J. West, and J. W. M. DuMond, Phys. Rev. 77, 475 (1950).

45. B. B. Kinsey, Canadian J. Research 26A, 404 (1948); ibid, 26A, 421 (1948).

46. L. M. Langer and R. D. Moffat, Phys. Rev. 78, 74 (1950).

47. R. B. Heller, E. F. Strucker, and A. H. Weber, Rev. Sci. Inst. 21, 898 (1950).

48. W. W. T. Crane, private communication.

49. A.C.Price, J.W.Motz, and L.M.Langer, Phys. Rev. 77, 744 (1950); loc. cit., 798.

50. F. Asaro and I. Perlman, private communication (March, 1950).

51. R. A. James, A. E. Florin, H. H. Hopkins, and A. Ghiorso, The Transuranium Elements: Research Papers, National Nuclear Energy

Series, Plutonium Project Record 14B, Paper No. 22.8, New York: McGraw - Hill Book Company, Inc. (1949).

52. D. A. Orth and G. D. O'Kelley, to be published.

53. W. W. T. Crane, A. Ghiorso, and I. Perlman, to be published.

54. R. A. James and A. Ghiorso, to be published.

55. G. D. O'Kelley, G. W. Barton, Jr., W. W. T. Crane, and I. Perlman, Phys. Rev. 80, 293 (1950).

56. A. H. Jaffey and J. Lerner, Argonne National Laboratory Report ANL-4411 (February 13, 1950).

57. W. Thiel and A. H. Jaffey, Argonne National Laboratory Report ANL-4370 (November 23, 1949).

58. J. C. Sullivan, G. L. Pyle, M. H. Studier, P. R. Fields, and W. M. Manning, Argonne National Laboratory Report ANL-4502 (September 12, 1950); Phys. Rev., to be published.

59. S. G. Thompson, K. Street, Jr., A. Ghiorso, and F. L. Reynolds, University of California Radiation Laboratory Report UCRL-956 (November, 1950); Phys. Rev. to be published.

60. A. Ghiorso, private communication.

61. H. Slätis and K. Siegbahn, Phys. Rev. 75, 318 (1949).

62. A. L. Lutz, M. L. Pool, and J. D. Kurbatov, Phys. Rev. 65, 61 (1944).

63. K. Siegbahn, Phil. Mag. 37, 162 (1946); Proc. Roy. Soc. 188A, 541 (1946).

64. J. A. Harvey, Phys. Rev. 81, 333 (1951).

65. H. M. Neumann, University of California Radiation Laboratory Report MB-IP No. 484.

66. B.B.Kinsey, G.A.Bartholomew, and W.H. Walker, Phys. Rev. 78, 77 (1950).

67. E. K. Hyde and G. D. O'Kelley, University of California Radiation Laboratory Report UCRL-1064 (December 28, 1950); Phys. Rev., to be published.

68. B. E. Robertson, W. E. Scott, and M. L. Pool, Phys. Rev. 76, 1649 (1949).

69. L. M. Langer and H. C. Price, Jr., Phys. Rev. 76, 641 (1941).

70. L. G. Mann and P. Axel, Phys. Rev. 80, 759 (1950).

71. R. Overstreet, L. J. Jacobson, and J. G. Hamilton, Manhattan Project Metallurgical Laboratory Report CH-498 (February 15, 1943).

72. S. V. Castner, unpublished data.

73. E. J. Konopinski and G. E. Uhlenbeck, Phys. Rev. 60, 308 (1941).

74. E. J. Konopinski, Revs. Modern Phys. 15, 209 (1943).